IOP Publishing | Royal Swedish Academy of Sciences Physica Scripta
Phys. Scr. 89 (2014) 115403 (21pp) doi:10.1088/0031-8949/89/11/115403

Extended and revised analysis of singly ionized tin: Sn II

K Haris[1], **A Kramida**[2] **and A Tauheed**[1]

[1] Department of Physics, Aligarh Muslim University, Aligarh 202002, India
[2] National Institute of Standards and Technology, Gaithersburg, MD 20899, USA

E-mail: alexander.kramida@nist.gov

Received 2 December 2013, revised 21 May 2014
Accepted for publication 28 August 2014
Published 28 October 2014

Abstract

The electronic structure of singly ionized tin (Sn II) is partly a one-electron and partly a three-electron system with ground configuration $5s^25p$. The excited configurations are of the type $5s^2n\ell$ in the one-electron part, and $5s5p^2$, $5p^3$ and $5s5pn\ell$ ($n\ell = 6s$, 5d) in the three-electron system with quartet and doublet levels. The spectrum analyzed in this work was recorded on a 3 m normal incidence vacuum spectrograph of the Antigonish laboratory (Canada) in the wavelength region 300 Å–2080 Å using a triggered spark source. The existing interpretation of the one-electron level system was confirmed in this paper, while the $^2S_{1/2}$ level of the $5s5p^2$ configuration has been revised. The analysis has been extended to include new configurations $5p^3$, 5s5p5d and 5s5p6s with the aid of superposition-of-configurations Hartree–Fock calculations with relativistic corrections. The ionization potential obtained from the ng series was found to be 118 023.7(7) cm^{-1} (14.633 07(8) eV). We give a complete set of critically evaluated data on energy levels, observed wavelengths and transition probabilities of Sn II in the range 888–10 740 Å involving excitation of the $n = 5$ electrons.

S Online supplementary data available from stacks.iop.org/PS/89/115403/mmedia

Keywords: singly ionized tin, energy levels, classified lines, transition probabilities, ionization energy

(Some figures may appear in colour only in the online journal)

1. Introduction

Accurate data on the spectrum of singly ionized tin are needed in different fields of scientific research and industry. Such data are useful for astrophysical observations, development of various light sources, and for plasma diagnostics in fusion power plants. The astrophysical importance of tin has increased since gas-phase tin was first detected by Hobbs *et al* [1] in the spectra acquired with the Goddard High Resolution Spectrograph on board the *Hubble Space Telescope*. They observed the absorption line of Sn II at 1400.45 Å from various interstellar sources. Later, the same line was observed in diffuse interstellar clouds by Sofia *et al* [2]. They discovered that the gas-phase abundance of Sn in the interstellar medium (ISM) appears to be supersolar, which further substantiates the slow neutron capture (s-process) enrichment believed to be a major contributor to the nucleosynthesis of elements beyond the iron peak in the ISM. In erosion probing of vessel wall tiles of future fusion power plants, such as ITER, spectroscopic data on tin may play a major diagnostic role [3].

Singly ionized tin (Sn II) is the second member of the In I isoelectronic sequence with the ground configuration $4d^{10}5s^25p$ consisting of the ground level $^2P°_{1/2}$ and first excited level $^2P°_{3/2}$. The currently available spectroscopic information on Sn II compiled in Moore's Atomic Energy Levels (AEL) compilation [4] and listed in the Atomic Spectra Database (ASD) [5] of the National Institute of Standards and Technology (NIST) is based on an unpublished work of Shenstone. Prior to AEL, extensive work in this spectrum was carried out by McCormick and Sawyer [6], who revised the earlier findings of Green and Loring [7], Narayan and Rao [8], and Lang [9]. Shenstone in his work quoted in AEL re-investigated this spectrum in the wavelength range of

600–2500 Å and extended the analysis to include the 5s5p5d and 5s5p6s configurations. Shenstone revised some energy levels of Sn II and improved the accuracy of the earlier reported energy level values on the basis of his observations. Some spectral lines of Sn II were also reported by Brill [10] in his doctoral thesis and by Wu [11] in his master's thesis. Apart from spectroscopy of valence-shell electrons, spectral studies of the 4d-core excitation of Sn II in the extreme ultraviolet region with the dual laser plasma method were made by Lysaght *et al* [12] and by Duffy *et al* [13].

Despite those extensive studies, the currently available data are still inadequate, since there are considerable anomalies in energy level values and line assignments. Many of the energy levels given in AEL [4] are not supported by any published line lists. The lines determining these energy levels have to be re-discovered.

There are many theoretical studies on radiative lifetimes, transition rates, and oscillator strengths of Sn II. Among them, the most accurate and reliable calculation of oscillator strengths was made by Oliver and Hibbert [14]. Schectman *et al* [15] improved the earlier lifetime measurements of Andersen and Lindgård [16] and, by combining them with measured branching fractions, determined *f*-values for several transitions. Data from [16] were used by Sofia *et al* [2] to derive the gas-phase interstellar abundance of tin in several diffuse clouds.

In the present work, our motivation is to provide a comprehensive spectroscopic analysis of singly ionized tin on the basis of tin spectra taken by us, the tin spectral line list given by Wu [11], the Sn II spectral classification by McCormick and Sawyer [6], and lines reported by Brill [10]. All previously reported energy levels of this spectrum are subjected to a critical investigation. One of our goals is to resolve the questions in Moore's assignments of the $5s5p^2\ ^2S_{1/2}$ and $^2P_{1/2}$ levels [4]. Excitation from the $5s5p^2$ configuration to 5s5p(5d + 6s) and $5p^3$ is studied extensively in this work. Although some of the levels of these highly-excited configurations were tentatively identified by Shenstone and listed in AEL [4], Shenstone's analysis was incomplete in many respects. Some of the level values were given with question marks, and some had uncertain *J* values and/or designations. A very recent study carried out by Alonso-Medina *et al* [17] using laser-produced plasma of a Sn/Pb target reproduced some of the levels reported in AEL [4], but the majority of their suggested 5s5p5d and $5p^3$ level assignments and line classifications are made on the basis of a physically inadequate theoretical atomic model. For example, the spin–orbit coupling parameter ζ_{5p} should be approximately the same in all $n = 5$ configurations. However, the values reported in [17] vary from 745 cm^{-1} for 5s5p5d to 29 667 cm^{-1} for $5p^3$. We attempt to resolve all these questions in the present analysis. Interestingly, many of the 5s5p5d and $5p^3$ levels are located above the first ionization limit. Therefore, only those levels that have autoionization rates comparable to or smaller than the radiative decay rate were observed via their corresponding photon decay channel.

Although, as noted above, some studies of the 4d core-excited spectrum of Sn II have been published [12, 13], we restrict the scope of this paper to excitations of the $n = 5$ electrons.

2. Experimental details

The tin ions/atoms were excited by means of a triggered spark source, which consists of a 14.5 μF fast-charging low-inductance capacitor, chargeable up to 20 kV, and a trigger module to initiate the discharge in vacuum. Either pure electrodes made of tin, or tin samples inserted into a cavity in aluminum electrodes were used. The tin spectrum was recorded at St. Francis Xavier University, Antigonish (Canada) using a 3 m normal incidence vacuum ultraviolet (VUV) spectrograph in the (300–2080) Å wavelength region. A holographic osmium-coated grating with 2400 lines mm^{-1} was used to obtain reciprocal linear dispersion of about 1.4 Å mm^{-1} in the aforementioned region in the first order of diffraction. At least four or five different tracks of spectrum were photographed on Kodak SWR[3] (short-wave radiation) plates with varied experimental conditions, such as electric current and voltage. The purpose of the different exposures was to distinguish the lines of Sn II from other ionization species. This was achieved by inserting a low, medium, or high inductance in series with the spark circuit or by varying the charging potential within the limits of 2 kV and 6 kV. The inductances were made of copper wire, 2 mm in diameter, wound on a cylinder of diameter 24 cm in turns separated by about 4 mm. A low inductance coil had eight or nine turns of wire, a medium one had 25 turns, and the high inductance one had 40–50 turns. The optimal conditions for observing the Sn II spectrum were found to be at 2 kV without an additional inductance or at 4 kV with a medium inductance. Relative positions of spectral lines on the plates were measured using a Zeiss Abbe1 comparator at the Aligarh University (India). For their wavelength reduction, we used as internal standards the known impurity lines of C II [18, 19], C III [18, 20, 21], C IV [22], N II [18], O II [23], O III [24], O IV [25], Al II [18, 26], Al III [18, 22], Si II [18, 22], Si III [27], and Si IV [22]. The measured positions of the reference lines on the plates were fitted with second or third degree polynomials to obtain corrections to the dispersion curve. The standard deviation of the fits varied from 0.003 Å to 0.007 Å for different spectral regions and different plates. The mean value of 0.005 Å represents a rough estimate of the wavelength uncertainty of our measurements for sharp and unperturbed lines. A more detailed discussion of uncertainties is given in the next section.

3. Measurement uncertainties

The rough estimate of uncertainty given in the previous section, 0.005 Å for strong unperturbed lines, is insufficient

[3] Commercial products are identified in this paper for adequate specification of the experimental procedure. This identification does not imply recommendation or endorsement by NIST.

Table 1. Classified lines in Sn II.

I_{obs}[a] arb. u.	Char.[b]	λ_{obs}[c] Å	σ_{obs} cm^{-1}	λ_{Ritz}[d] Å	$\delta\lambda_{O-Ritz}$[e] Å	Classification				E_{low} cm^{-1}	E_{upp} cm^{-1}	A[f] s^{-1}	Acc[g]	Line Ref.[h]	TP Ref.[h]
1400		888.313(19)	112 572.9	888.304(4)	0.009	$5s^25p$	$^2P^\circ_{1/2}$	$5s^211d$	$^2D_{3/2}$	0.00	112 574.1			Wu	
3400		899.884(19)	111 125.4	899.907(10)	−0.023	$5s^25p$	$^2P^\circ_{1/2}$	$5s^210d$	$^2D_{3/2}$	0.00	111 122.6			Wu	
7300		917.378(6)	109 006.3	917.380(4)	−0.002	$5s^25p$	$^2P^\circ_{1/2}$	$5s^29d$	$^2D_{3/2}$	0.00	109 006.1	9.+7	E	TW	TW
3500		922.856(19)	108 359.3	922.870(3)	−0.014	$5s^25p$	$^2P^\circ_{1/2}$	$5s^210s$	$^2S_{1/2}$	0.00	108 357.6	2.4+7	E	Wu	TW
3700		923.01(4)	108 341	922.974(10)	0.04	$5s^25p$	$^2P^\circ_{3/2}$	$5s^211d$	$^2D_{5/2}$	4251.494	112 596.9			MS	
5800		935.571(19)	106 886.6	935.525(10)	0.046	$5s^25p$	$^2P^\circ_{3/2}$	$5s^210d$	$^2D_{5/2}$	4251.494	111 143.3			Wu	
14 000		945.802(6)	105 730.4	945.794(3)	0.008	$5s^25p$	$^2P^\circ_{1/2}$	$5s^28d$	$^2D_{3/2}$	0.00	105 731.3	1.5+8	E	TW	TW
12 000		954.440(6)	104 773.5	954.4332(14)	0.007	$5s^25p$	$^2P^\circ_{3/2}$	$5s^29d$	$^2D_{5/2}$	4251.494	109 025.72	9.+7	E	TW	TW
6200		954.614(6)	104 754.4	954.612(4)	0.002	$5s^25p$	$^2P^\circ_{3/2}$	$5s^29d$	$^2D_{3/2}$	4251.494	109 006.1	1.8+7	E	TW	TW
6900		955.299(6)	104 679.3	955.3068(10)	−0.008	$5s^25p$	$^2P^\circ_{1/2}$	$5s^29s$	$^2S_{1/2}$	0.00	104 678.41	3.9+7	E	TW	TW
2400		960.545(19)	104 107.6	960.558(4)	−0.013	$5s^25p$	$^2P^\circ_{3/2}$	$5s^210s$	$^2S_{1/2}$	4251.494	108 357.6	4.+7	E	Wu	TW
18 000		985.110(6)	101 511.5	985.1117(23)	−0.002	$5s^25p$	$^2P^\circ_{3/2}$	$5s^28d$	$^2D_{5/2}$	4251.494	105 762.82	1.6+8	E	TW	TW
10 000		985.411(19)	101 480.5	985.418(3)	−0.007	$5s^25p$	$^2P^\circ_{3/2}$	$5s^28d$	$^2D_{3/2}$	4251.494	105 731.3	3.0+7	E	Wu	TW
8600		995.742(6)	100 427.6	995.7490(10)	−0.007	$5s^25p$	$^2P^\circ_{3/2}$	$5s^29s$	$^2S_{1/2}$	4251.494	104 678.41	7.+7	E	TW	TW
19 000		997.168(6)	100 284.0	997.1669(5)	0.001	$5s^25p$	$^2P^\circ_{1/2}$	$5s^27d$	$^2D_{3/2}$	0.00	100 284.111	2.8+8	D+	TW	TW
16 000		1016.238(6)	98 402.1	1016.2353(5)	0.003	$5s^25p$	$^2P^\circ_{1/2}$	$5s^28s$	$^2S_{1/2}$	0.00	98 402.412	7.+7	E	TW	TW
24 000		1040.720(6)	96 087.3	1040.71 860(19)	0.001	$5s^25p$	$^2P^\circ_{3/2}$	$5s^27d$	$^2D_{5/2}$	4251.494	100 338.947	3.0+8	D+	TW	TW
16 000		1041.313(6)	96 032.6	1041.31 287(19)	0.000	$5s^25p$	$^2P^\circ_{3/2}$	$5s^27d$	$^2D_{3/2}$	4251.494	100 284.111	6.+7	E	TW	TW
25 000		1062.123(7)	94 151.1	1062.12453(17)	−0.002	$5s^25p$	$^2P^\circ_{3/2}$	$5s^28s$	$^2S_{1/2}$	4251.494	98 402.412	1.3+8	E	TW	TW
43 000		1108.138(10)	90 241.5	1108.1369(6)	0.001	$5s^25p$	$^2P^\circ_{1/2}$	$5s^26d$	$^2D_{3/2}$	0.00	90 241.554	4.7+8	B+	TW	OH10
53 000		1159.014(10)	86 280.2	1159.0129(6)	0.001	$5s^25p$	$^2P^\circ_{1/2}$	$5s^27s$	$^2S_{1/2}$	0.00	86 280.318	1.01+8	C+	TW	OH10
74 000		1161.434(10)	86 100.5	1161.43479(20)	−0.001	$5s^25p$	$^2P^\circ_{3/2}$	$5s^26d$	$^2D_{5/2}$	4251.494	90 351.894	5.5+8	B+	TW	OH10
56 000		1162.926(10)	85 990.0	1162.92511(20)	0.001	$5s^25p$	$^2P^\circ_{3/2}$	$5s^26d$	$^2D_{3/2}$	4251.494	90 241.554	1.28+8	B+	TW	OH10
37 000	bl(Sn IV)	1185.675(14)	84 340.1	1185.684(5)	−0.009	$5s5p^2$	$^4P_{3/2}$	$5s5p(^1P^\circ)5d$	$^2D^\circ_{5/2}$	48 368.185	132 707.7			TW	
66 000	bl(Si II)	1193.299(14)	83 801.3	1193.308(3)	−0.009	$5s5p^2$	$^4P_{3/2}$	$5s5p(^1P^\circ)5d$	$^2D^\circ_{3/2}$	48 368.185	132 168.83			TW	
91 000		1219.088(10)	82 028.3	1219.08367(22)	0.004	$5s^25p$	$^2P^\circ_{3/2}$	$5s^27s$	$^2S_{1/2}$	4251.494	86 280.318	3.35+8	B+	TW	OH10
100 000		1223.715(10)	81 718.4	1223.716(5)	−0.001	$5s^25p$	$^2P^\circ_{1/2}$	$5s5p^2$	$^2P_{3/2}$	0.00	81 718.3	4.08+8	B+	TW	OH10
110 000		1242.928(10)	80 455.2	1242.929(7)	−0.001	$5s^25p$	$^2P^\circ_{1/2}$	$5s5p^2$	$^2P_{1/2}$	0.00	80 455.1	4.5+8	B+	TW	OH10
31 000		1285.659(7)	77 781.1	1285.655(3)	0.004	$5s5p^2$	$^4P_{1/2}$	$5s5p(^3P^\circ)5d$	$^4P^\circ_{3/2}$	46 464.290	12 4245.66			TW	
200 000		1290.871(10)	77 467.1	1290.875(5)	−0.004	$5s^25p$	$^2P^\circ_{3/2}$	$5s5p^2$	$^2P_{3/2}$	4251.494	81 718.3	2.95+9	B+	TW	OH10
37 000	H	1303.902(14)	76 692.9	1303.912(7)	−0.010	$5s5p^2$	$^4P_{1/2}$	5p3	$^4S^\circ_{3/2}$	46 464.290	123 156.6	9.+8	D+	TW	TW
210 000		1312.275(10)	76 203.5	1312.274(7)	0.001	$5s^25p$	$^2P^\circ_{3/2}$	$5s5p^2$	$^2P_{1/2}$	4251.494	80 455.1	1.77+9	B+	TW	OH10
100 000	bl(Sn III)	1313.087(14)	76 156.4	1313.087(14)		$5s5p^2$	$^4P_{3/2}$	$5s5p(^3P^\circ)5d$	$^4P^\circ_{1/2}$	48 368.185	124 524.6	2.0+9	D+	TW	TW
210 000		1316.572(10)	75 954.8	1316.581(6)	−0.009	$5s^25p$	$^2P^\circ_{1/2}$	$5s5p^2$	$^2S_{1/2}$	0.00	75 954.3	2.14+9	B+	TW	OH10
86 000		1317.907(7)	75 877.9	1317.914(3)	−0.007	$5s5p^2$	$^4P_{3/2}$	$5s5p(^3P^\circ)5d$	$^4P^\circ_{3/2}$	48 368.185	124 245.66	1.3+9	D+	TW	TW
33 000	H	1327.669(14)	75 320.0	1327.668(10)	0.001	$5s5p^2$	$^4P_{3/2}$	$5s5p(^3P^\circ)5d$	$^4P^\circ_{5/2}$	48 368.185	123 688.2			TW	
67 000	h	1337.103(14)	74 788.6	1337.105(7)	−0.002	$5s5p^2$	$^4P_{3/2}$	5p3	$^4S^\circ_{3/2}$	48 368.185	123 156.6	1.3+9	D+	TW	TW
13 000	h	1353.843(14)	73 863.8	1353.848(6)	−0.005	$5s5p^2$	$^2D_{3/2}$	$5s5p(^1P^\circ)5d$	$^2D^\circ_{5/2}$	58 844.181	132 707.7	3.6+8	D+	TW	TW
58 000	h	1358.707(14)	73 599.4	1358.695(10)	0.012	$5s5p^2$	$^4P_{1/2}$	$5s5p(^3P^\circ)5d$	$^4D^\circ_{3/2}$	46 464.290	120 064.3	1.9+9	D+	TW	TW
200 000	H,bl(Sn III)*	1360.226(20)	73 517.2	1360.259(4)	−0.033	$5s5p^2$	$^4P_{5/2}$	$5s5p(^3P^\circ)5d$	$^4P^\circ_{3/2}$	50 730.224	124 245.66	7.5+8	D+	TW	TW
120 000	H,bl(Sn III)*	1360.226(20)	73 517.2	1360.233(12)	−0.007	$5s5p^2$	$^4P_{1/2}$	$5s5p(^3P^\circ)5d$	$^4D^\circ_{1/2}$	46 464.290	119 981.1	3.3+9	D+	TW	TW
93 000		1363.799(7)	73 324.6	1363.798(4)	0.001	$5s5p^2$	$^2D_{3/2}$	$5s5p(^1P^\circ)5d$	$^2D^\circ_{3/2}$	58 844.181	132 168.83	3.6+9	D+	TW	TW
100 000	h	1365.282(14)	73 244.9	1365.295(6)	−0.013	$5s5p^2$	$^2D_{5/2}$	$5s5p(^1P^\circ)5d$	$^2D^\circ_{5/2}$	59 463.481	132 707.7	3.4+9	D+	TW	TW
100 000	h,bl(Sn III)	1370.651(14)	72 958.0	1370.652(10)	−0.001	$5s5p^2$	$^4P_{5/2}$	$5s5p(^3P^\circ)5d$	$^4P^\circ_{5/2}$	50 730.224	123 688.2	2.1+9	D+	TW	TW
46 000		1375.416(7)	72 705.3	1375.415(5)	0.001	$5s5p^2$	$^2D_{5/2}$	$5s5p(^1P^\circ)5d$	$^2D^\circ_{3/2}$	59 463.481	132 168.83	1.8+8	D+	TW	TW
68 000	h	1380.704(14)	72 426.8	1380.712(7)	−0.008	$5s5p^2$	$^4P_{5/2}$	5p3	$^4S^\circ_{3/2}$	50 730.224	123 156.6	2.3+9	D+	TW	TW
130 000	s	1391.100(7)	71 885.6	1391.103(5)	−0.003	$5s5p^2$	$^4P_{3/2}$	$5s5p(^3P^\circ)5d$	$^4D^\circ_{5/2}$	48 368.185	120 253.6	2.3+9	D+	TW	TW
130 000	H,bl(Sn IV)	1393.510(20)	71 761.2	1393.510(20)		$5s5p^2$	$^4P_{5/2}$	$5s5p(^3P^\circ)5d$	$^4D^\circ_{7/2}$	50 730.224	122 491.5	3.1+9	D+	TW	TW
62 000		1394.667(19)	71 701.7	1394.646(7)	0.021	$5s^25p$	$^2P^\circ_{3/2}$	$5s5p^2$	$^2S_{1/2}$	4251.494	75 954.3	7.+6	E	Wu*	OH10
19 000	h	1394.764(14)	71 696.7	1394.776(10)	−0.012	$5s5p^2$	$^4P_{3/2}$	$5s5p(^3P^\circ)5d$	$^4D^\circ_{3/2}$	48 368.185	120 064.3	1.0+9	D+	TW	TW
15 000	H	1396.399(14)	71 612.8	1396.396(13)	0.003	$5s5p^2$	$^4P_{3/2}$	$5s5p(^3P^\circ)5d$	$^4D^\circ_{1/2}$	48 368.185	119 981.1	2.4+8	D+	TW	TW
360 000		1400.454(20)	71 405.4	1400.4398(9)	0.014	$5s^25p$	$^2P^\circ_{1/2}$	$5s^25d$	$^2D_{3/2}$	0.00	71 406.142	2.05+9	B+	TW	OH10
5000		1438.365(14)	69 523.4	1438.365(6)	0.000	$5s5p^2$	$^4P_{5/2}$	$5s5p(^3P^\circ)5d$	$^4D^\circ_{5/2}$	50 730.224	120 253.6			TW	
530 000		1474.995(20)	67 796.8	1474.9966(3)	−0.002	$5s^25p$	$^2P^\circ_{3/2}$	$5s^25d$	$^2D_{5/2}$	4251.494	72 048.260	1.95+9	B+	TW	OH10
15 000		1481.747(7)	67 487.9	1481.742(5)	0.005	$5s5p^2$	$^4P_{1/2}$	$5s5p(^3P^\circ)6s$	$^2P^\circ_{1/2}$	46 464.290	113 952.44			TW	
79 000		1489.091(10)	67 155.1	1489.1002(4)	−0.009	$5s^25p$	$^2P^\circ_{3/2}$	$5s^25d$	$^2D_{3/2}$	4251.494	71 406.142	1.59+8	B+	TW	OH10
32 000		1495.037(7)	66 888.0	1495.037(7)		$5s5p^2$	$^4P_{3/2}$	$5s5p(^3P^\circ)5d$	$^4F^\circ_{5/2}$	48 368.185	115 256.2	1.1+8	D+	TW	TW
33 000		1517.961(7)	65 877.8	1517.967(5)	−0.006	$5s5p^2$	$^4P_{3/2}$	$5s5p(^3P^\circ)6s$	$^4P^\circ_{5/2}$	48 368.185	114 245.75	4.4+8	D+	TW	TW

Table 1. (Continued.)

I_{obs}[a] arb. u.	Char.[b]	λ_{obs}[c] Å	σ_{obs} cm^{-1}	λ_{Ritz}[d] Å	$\delta\lambda_{O-Ritz}$[e] Å	Classification				E_{low} cm^{-1}	E_{upp} cm^{-1}	A[f] s^{-1}	Acc[g]	Line Ref.[h]	TP Ref.[h]
24 000	H,bl(Sn)	1522.206(20)	65 694.1	1522.235(7)	−0.029	$5s5p^2$	$^4P_{5/2}$	$5s5p(^3P^\circ)5d$	$^4F^\circ_{7/2}$	50 730.224	116 423.1	8.3+7	D+	TW	TW
15 000	H,bl(Sn)	1527.856(14)	65 451.2	1527.873(5)	−0.017	$5s5p^2$	$^4P_{3/2}$	$5s5p(^3P^\circ)5d$	$^2D^\circ_{5/2}$	48 368.185	113 818.65			TW	
14 000		1543.653(19)	64 781.4	1543.634(5)	0.019	$5s5p^2$	$^2D_{5/2}$	$5s5p(^3P^\circ)5d$	$^4P^\circ_{3/2}$	59 463.481	124 245.66			Wu*	
60 000		1554.881(14)	64 313.6	1554.896(5)	−0.015	$5s5p^2$	$^4P_{1/2}$	$5s5p(^3P^\circ)6s$	$^4P^\circ_{3/2}$	46 464.290	110 777.28	4.0+8	D+	TW	TW
13 000		1570.056(19)	63 692.0	1570.028(10)	0.028	$5s5p^2$	$^2D_{5/2}$	5p3	$^4S^\circ_{3/2}$	59 463.481	123 156.6			Wu*	
33 000		1574.426(8)	63 515.2	1574.418(5)	0.008	$5s5p^2$	$^4P_{5/2}$	$5s5p(^3P^\circ)6s$	$^4P^\circ_{5/2}$	50 730.224	114 245.75	7.2+8	D+	TW	TW
14 000	H,bl(Sn)	1585.071(16)	63 088.7	1585.077(5)	−0.006	$5s5p^2$	$^4P_{5/2}$	$5s5p(^3P^\circ)5d$	$^2D^\circ_{5/2}$	50 730.224	113 818.65	6.2+7	D+	TW	TW
9200		1587.532(19)	62 990.9	1587.571(7)	−0.039	$5s5p^2$	$^4P_{1/2}$	$5s5p(^3P^\circ)6s$	$^4P^\circ_{1/2}$	46 464.290	109 453.6	1.5+8	D+	Wu	TW
15 000	H,bl(Sn)	1593.418(16)	62 758.2	1593.414(7)	0.004	$5s5p^2$	$^4P_{1/2}$	$5s^2 10p$	$^2P^\circ_{1/2}$	46 464.290	109 222.6			TW	
16 000		1602.325(12)	62 409.3	1602.331(5)	−0.006	$5s5p^2$	$^4P_{3/2}$	$5s5p(^3P^\circ)6s$	$^4P^\circ_{3/2}$	48 368.185	110 777.28	1.1+8	D+	TW	TW
22 000	bl(Sn III)	1628.422(16)	61 409.1	1628.415(7)	0.007	$5s5p^2$	$^2D_{3/2}$	$5s5p(^3P^\circ)5d$	$^4D^\circ_{5/2}$	58 844.181	120 253.6			TW	
16 000		1637.059(8)	61 085.2	1637.052(7)	0.007	$5s5p^2$	$^4P_{3/2}$	$5s5p(^3P^\circ)6s$	$^4P^\circ_{1/2}$	48 368.185	109 453.6	6.6+8	D+	TW	TW
8100		1643.262(12)	60 854.6	1643.266(7)	−0.004	$5s5p^2$	$^4P_{3/2}$	$5s^2 10p$	$^2P^\circ_{1/2}$	48 368.185	109 222.6	1.4+8	D+	TW	TW
6300		1648.562(12)	60 658.9	1648.548(9)	0.014	$5s^2 5d$	$^2D_{5/2}$	$5s5p(^1P^\circ)5d$	$^2D^\circ_{5/2}$	72 048.260	132 707.7			TW	
19 000		1665.364(8)	60 046.9	1665.361(6)	0.003	$5s5p^2$	$^4P_{5/2}$	$5s5p(^3P^\circ)6s$	$^4P^\circ_{3/2}$	50 730.224	110 777.28	3.8+8	D+	TW	TW
21 000		1699.418(16)	58 843.7	1699.4034(13)	0.015	$5s^2 5p$	$^2P^\circ_{1/2}$	$5s5p^2$	$^2D_{3/2}$	0.00	58 844.181	2.99+7	B+	TW	OH10
1700		1755.621(19)	56 959.9	1755.630(9)	−0.009	$5s5p^2$	$^2D_{5/2}$	$5s5p(^3P^\circ)5d$	$^4F^\circ_{7/2}$	59 463.481	116 423.1			Wu*	
15 000		1757.893(16)	56 886.3	1757.8905(14)	0.002	$5s^2 5p$	$^2P^\circ_{1/2}$	$5s^2 6s$	$^2S_{1/2}$	0.00	56 886.363	3.04+8	B+	TW	OH10
6500		1778.898(16)	56 214.6	1778.900(12)	−0.002	$5s5p^2$	$^2S_{1/2}$	$5s5p(^1P^\circ)5d$	$^2D^\circ_{3/2}$	75 954.3	132 168.83			TW	
1900		1805.002(19)	55 401.6	1805.003(7)	−0.001	$5s5p^2$	$^2D_{3/2}$	$5s5p(^3P^\circ)6s$	$^4P^\circ_{5/2}$	58 844.181	114 245.75			Wu	
14 000		1811.197(16)	55 212.1	1811.2009(5)	−0.004	$5s^2 5p$	$^2P^\circ_{3/2}$	$5s5p^2$	$^2D_{5/2}$	4251.494	59 463.481	6.4+7	B+	TW	OH10
1100		1814.602(12)	55 108.5	1814.610(8)	−0.008	$5s5p^2$	$^2D_{3/2}$	$5s5p(^3P^\circ)6s$	$^2P^\circ_{1/2}$	58 844.181	113 952.44			TW	
1500		1819.039(12)	54 974.1	1819.026(7)	0.013	$5s5p^2$	$^2D_{3/2}$	$5s5p(^3P^\circ)5d$	$^2D^\circ_{5/2}$	58 844.181	113 818.65			TW	
11 000		1831.757(16)	54 592.4	1831.7472(5)	0.010	$5s^2 5p$	$^2P^\circ_{3/2}$	$5s5p^2$	$^2D_{3/2}$	4251.494	58 844.181	2.2+7	C+	TW	OH10
370		1855.604(19)	53 890.8	1855.600(7)	0.004	$5s^2 6s$	$^2S_{1/2}$	$5s5p(^3P^\circ)6s$	$^4P^\circ_{3/2}$	56 886.363	110 777.28			Wu	
570		1886.107(8)	53 019.26	1886.110(6)	−0.003	$5s5p^2$	$^4P_{3/2}$	$5s^2 8p$	$^2P^\circ_{3/2}$	48 368.185	101 387.37			TW	
7200		1899.901(16)	52 634.3	1899.8812(5)	0.020	$5s^2 5p$	$^2P^\circ_{3/2}$	$5s^2 6s$	$^2S_{1/2}$	4251.494	56 886.363	5.6+8	B+	TW	OH10
170		2108.475(19)	47 412.6	2108.493(12)	−0.018	$5s5p^2$	$^2D_{3/2}$	$5s^2 9p$	$^2P^\circ_{1/2}$	58 844.181	106 256.4			Wu	
250		2131.208(19)	46 906.9	2131.218(18)	−0.010	$5s5p^2$	$^2D_{5/2}$	$5s^2 9p$	$^2P^\circ_{3/2}$	59 463.481	106 370.2			Wu	
720	bl(Sn III)	2148.61(8)	46 527.1	2148.589(16)	0.02	$5s5p^2$	$^2D_{3/2}$	$5s^2 6f$	$^2F^\circ_{5/2}$	58 844.181	105 371.7			MS	
520		2150.8442(9)	46 478.749	2150.8451(7)	−0.0009	$5s^2 5p$	$^2P^\circ_{3/2}$	$5s5p^2$	$^4P_{5/2}$	4251.494	50 730.224	4.0+5	D+	Brill	OH10
530		2151.5135(20)	46 464.29	2151.5136(20)	−0.0001	$5s^2 5p$	$^2P^\circ_{1/2}$	$5s5p^2$	$^4P_{1/2}$	0.00	46 464.290	2.1+6	C+	Brill	OH10
160		2200.075(19)	45 438.8	2200.0341(11)	0.041	$5s5p^2$	$^4P_{1/2}$	$5s^2 7p$	$^2P^\circ_{1/2}$	46 464.290	91 903.945			Wu	
	m(Sn I)			2246.443(8)		$5s^2 6s$	$^2S_{1/2}$	$5s^2 8p$	$^2P^\circ_{3/2}$	56 886.363	101 387.37			MS	
67		2252.845(19)	44 374.6	2252.831(15)	0.014	$5s^2 5d$	$^2D_{5/2}$	$5s5p(^3P^\circ)5d$	$^4F^\circ_{7/2}$	72 048.260	116 423.1			Wu*	
35		2255.726(19)	44 317.9	2255.729(19)	−0.003	$5s^2 6s$	$^2S_{1/2}$	$5s^2 8p$	$^2P^\circ_{1/2}$	56 886.363	101 204.2			Wu	
260		2266.0156(10)	44 116.677	2266.0149(7)	0.0007	$5s^2 5p$	$^2P^\circ_{3/2}$	$5s5p^2$	$^4P_{3/2}$	42 51.494	48 368.185	4.3+5	D+	Brill	OH10
86		2296.293(19)	43 535.0	2296.2548(9)	0.038	$5s5p^2$	$^4P_{3/2}$	$5s^2 7p$	$^2P^\circ_{1/2}$	48 368.185	91 903.945			Wu	
45		2333.43(14)	42 842	2333.573(11)	−0.14	$5s^2 5d$	$^2D_{3/2}$	$5s5p(^3P^\circ)6s$	$^4P^\circ_{5/2}$	71 406.142	114 245.75			Wu	
120		2349.825(19)	42 543.3	2349.833(9)	−0.008	$5s5p^2$	$^2D_{3/2}$	$5s^2 8p$	$^2P^\circ_{3/2}$	58 844.181	101 387.37			Wu	
130		2350.698(19)	42 527.5	2350.708(16)	−0.010	$5s5p^2$	$^2P_{3/2}$	$5s5p(^3P^\circ)5d$	$^4P^\circ_{3/2}$	81 718.3	124 245.66			Wu	
	m			2357.074(12)		$5s^2 5d$	$^2D_{3/2}$	$5s5p(^3P^\circ)5d$	$^2D^\circ_{5/2}$	71 406.142	113 818.65			Wu	
	m			2359.995(21)		$5s5p^2$	$^2D_{3/2}$	$5s^2 8p$	$^2P^\circ_{1/2}$	58 844.181	101 204.2			Wu	
3700		2360.28(10)	42 355	2360.230(18)	0.05x	$5s^2 6d$	$^2D_{5/2}$	$5s5p(^1P^\circ)5d$	$^2D^\circ_{5/2}$	90 351.894	132 707.7			Wu*	
310		2368.2265(6)	42 212.795	2368.2265(6)	0.0000	$5s^2 5p$	$^2P^\circ_{3/2}$	$5s5p^2$	$^4P_{1/2}$	42 51.494	46 464.290	5.6+5	C+	Brill	OH10
48		2369.15(10)	42 196.4	2369.086(11)	0.06	$5s^2 5d$	$^2D_{5/2}$	$5s5p(^3P^\circ)6s$	$^4P^\circ_{5/2}$	72 048.260	114 245.75			Wu	
220		2384.565(19)	41 923.6	2384.548(9)	0.017	$5s5p^2$	$^2D_{5/2}$	$5s^2 8p$	$^2P^\circ_{3/2}$	59 463.481	101 387.37			Wu	
53		2393.309(19)	41 770.4	2393.311(12)	−0.002	$5s^2 5d$	$^2D_{5/2}$	$5s5p(^3P^\circ)5d$	$^2D^\circ_{5/2}$	72 048.260	113 818.65			Wu*	
85		2406.712(19)	41 537.8	2406.7088(6)	0.003	$5s5p^2$	$^4P_{5/2}$	$5s^2 7p$	$^2P^\circ_{3/2}$	50 730.224	92 268.106	3.4+5	D+	Wu	OH10
160	bl(Sn I)	2433.48(3)	41 080.9	2433.49(3)	−0.01	$5s^2 6p$	$^2P^\circ_{1/2}$	$5s^2 11d$	$^2D_{3/2}$	71 493.273	112 574.1			Wu	
5700	:	2442.7	40 926	2442.7019(6)		$5s5p^2$	$^4P_{3/2}$	$5s^2 4f$	$^2F^\circ_{5/2}$	48 368.185	89 294.055	2.4+5	D+	AM	OH10
3500		2448.9079(7)	40 822.163	2448.9089(4)	−0.0010	$5s5p^2$	$^2D_{3/2}$	$5s^2 5f$	$^2F^\circ_{5/2}$	58 844.181	99 666.327	6.4+7	D+	Brill	TW
2300	:	2486.6	40 203	2486.6356(5)		$5s5p^2$	$^2D_{5/2}$	$5s^2 5f$	$^2F^\circ_{5/2}$	59 463.481	99 666.327	1.0+7	D	AM	AM
4100		2486.9666(8)	40 197.495	2486.9665(4)	0.0001	$5s5p^2$	$^2D_{5/2}$	$5s^2 5f$	$^2F^\circ_{7/2}$	59 463.481	99 660.978	6.8+7	D+	Brill	TW
1700		2522.69(9)	39 628.3	2522.62(8)	0.07	$5s^2 6p$	$^2P^\circ_{1/2}$	$5s^2 10d$	$^2D_{3/2}$	71 493.273	111 122.6			MS	
1900		2538.95(10)	39 374.5	2539.169(13)	−0.22x	$5s^2 5d$	$^2D_{3/2}$	$5s5p(^3P^\circ)6s$	$^4P^\circ_{3/2}$	71 406.142	110 777.28			Wu	
190		2579.15(23)	38 761	2578.82(7)	0.33	$5s^2 6p$	$^2P^\circ_{3/2}$	$5s^2 10d$	$^2D_{5/2}$	72 377.4484	111 143.3	1.0+7	D+	MS	TW
550	:	2592.3	38 564	2592.3281(5)		$5s5p^2$	$^4P_{5/2}$	$5s^2 4f$	$^2F^\circ_{5/2}$	50 730.224	89 294.055	1.9+5	D+	AM	OH10

Table 1. (Continued.)

I_{obs}[a] arb. u.	Char.[b]	λ_{obs}[c] Å	σ_{obs} cm^{-1}	λ_{Ritz}[d] Å	$\delta\lambda_{O-Ritz}$[e] Å	Classification				E_{low} cm^{-1}	E_{upp} cm^{-1}	A[f] s^{-1}	Acc[g]	Line Ref.[h]	TP Ref.[h]
1200		2592.7198(17)	38 558.01	2592.7181(5)	0.0017	$5s5p^2$	$^4P_{5/2}$	$5s^24f$	$^2F^\circ_{7/2}$	50 730.224	89 288.255	2.9+6	C+	Brill	OH10
200		2608.74(24)	38 321	2608.74(24)		$5s^26p$	$^2P^\circ_{3/2}$	$5s^211s$	$^2S_{1/2}$	72 377.4484	110 699			MS	
880	bl(Sn III)	2643.56(3)	37 816.5	2643.564(19)	0.0	$5s^25d$	$^2D_{3/2}$	$5s^210p$	$^2P^\circ_{1/2}$	71 406.142	109 222.6			Wu	
860		2664.99(10)	37 512.4	2664.96(3)	0.03	$5s^26p$	$^2P^\circ_{1/2}$	$5s^29d$	$^2D_{3/2}$	71 493.273	109 006.1	1.4+7	D+	MS	TW
220		2711.86(3)	36 864.2	2711.85(3)	0.01	$5s^26p$	$^2P^\circ_{1/2}$	$5s^210s$	$^2S_{1/2}$	71 493.273	108 357.6			Wu	
400		2727.76(3)	36 649.3	2727.834(11)	−0.07	$5s^26p$	$^2P^\circ_{3/2}$	$5s^29d$	$^2D_{5/2}$	72 377.4484	109 025.72	1.6+7	D+	Wu	TW
180		2778.4(3)	35 982	2778.49(3)	−0.1	$5s^26p$	$^2P^\circ_{3/2}$	$5s^210s$	$^2S_{1/2}$	72 377.4484	108 357.6			MS	
240		2825.51(3)	35 381.4	2825.4849(7)	0.03	$5s^26s$	$^2S_{1/2}$	$5s^27p$	$^2P^\circ_{3/2}$	56 886.363	92 268.106	1.11+6	C+	Wu	OH10
210		2868.61(3)	34 849.9	2868.577(23)	0.03	$5s^25d$	$^2D_{3/2}$	$5s^29p$	$^2P^\circ_{1/2}$	71 406.142	106 256.4			Wu	
220		2912.82(10)	34 320.9	2912.74(3)	0.08	$5s^25d$	$^2D_{5/2}$	$5s^29p$	$^2P^\circ_{3/2}$	72 048.260	106 370.2			MS	
610		2919.86(3)	34 238.2	2919.87(3)	−0.01	$5s^26p$	$^2P^\circ_{1/2}$	$5s^28d$	$^2D_{3/2}$	71 493.273	105 731.3	2.4+7	D+	Wu	TW
190		2943.30(3)	33 965.5	2943.30(3)	0.00	$5s^25d$	$^2D_{3/2}$	$5s^26f$	$^2F^\circ_{5/2}$	71 406.142	105 371.7			Wu	
400		2949.54(3)	33 893.7	2949.533(17)	0.01	$5s^26d$	$^2D_{5/2}$	$5s5p(^3P^\circ)5d$	$^4P^\circ_{3/2}$	90 351.894	124 245.66			Wu	
220		2990.99(3)	33 424.0	2990.9965(8)	−0.01	$5s5p^2$	$^2D_{3/2}$	$5s^27p$	$^2P^\circ_{3/2}$	58 844.181	92 268.106	9.1+5	C+	Wu	OH10
790		2994.46(3)	33 385.3	2994.451(21)	0.01	$5s^26p$	$^2P^\circ_{3/2}$	$5s^28d$	$^2D_{5/2}$	72 377.4484	105 762.82	2.7+7	D+	Wu	TW
110		2997.1(3)	33 355	2997.28(3)	−0.2	$5s^26p$	$^2P^\circ_{3/2}$	$5s^28d$	$^2D_{3/2}$	72 377.4484	105 731.3			MS	
260		3012.41(5)	33 186.3	3012.519(9)	−0.11	$5s^26p$	$^2P^\circ_{1/2}$	$5s^29s$	$^2S_{1/2}$	71 493.273	104 678.41			Wu	
450		3023.92(3)	33 060.1	3023.9444(14)	−0.03	$5s5p^2$	$^2D_{3/2}$	$5s^27p$	$^2P^\circ_{1/2}$	58 844.181	91 903.945	7.8+6	C+	Wu	OH10
680		3047.44(3)	32 804.9	3047.4642(9)	−0.02	$5s5p^2$	$^2D_{5/2}$	$5s^27p$	$^2P^\circ_{3/2}$	59 463.481	92 268.106	6.8+6	B+	Wu	OH10
930		3094.68(11)	32 304.1	3094.985(9)	−0.30	$5s^26p$	$^2P^\circ_{3/2}$	$5s^29s$	$^2S_{1/2}$	72 377.4484	104 678.41			MS	
480		3101.25(16)	32 235.7	3101.40(4)	−0.15x	$5s5p^2$	$^2P_{3/2}$	$5s5p(^3P^\circ)6s$	$^2P^\circ_{1/2}$	81 718.3	113 952.44			Wu*	
15 000		3283.1399(9)	30 449.874	3283.1399(7)	0.0000	$5s5p^2$	$^2D_{3/2}$	$5s^24f$	$^2F^\circ_{5/2}$	58 844.181	89 294.055	1.70+8	B+	Brill	OH10
13 000	:	3351.3	29 830.6	3351.3021(8)		$5s5p^2$	$^2D_{5/2}$	$5s^24f$	$^2F^\circ_{5/2}$	59 463.481	89 294.055	1.21+7	B+	AM	OH10
13 000		3351.9523(12)	29 824.788	3351.9538(8)	−0.0015	$5s5p^2$	$^2D_{5/2}$	$5s^24f$	$^2F^\circ_{7/2}$	59 463.481	89 288.255	1.82+8	B+	Brill	OH10
87		3355.5(3)	29 793	3354.96(4)	0.5	$5s^25d$	$^2D_{3/2}$	$5s^28p$	$^2P^\circ_{1/2}$	71 406.142	101 204.2			MS	
350		3407.41(12)	29 339.4	3407.442(19)	−0.03	$5s^25d$	$^2D_{5/2}$	$5s^28p$	$^2P^\circ_{3/2}$	72 048.260	101 387.37			MS	
1700		3472.333(3)	28 790.837	3472.3329(12)	0.000	$5s^26p$	$^2P^\circ_{1/2}$	$5s^27d$	$^2D_{3/2}$	71 493.273	100 284.111	4.5+7	D+	Brill	TW
660		3537.47(13)	28 260.7	3537.5363(12)	−0.07	$5s^25d$	$^2D_{3/2}$	$5s^25f$	$^2F^\circ_{5/2}$	71 406.142	99 666.327	3.6+6	D	MS	AM
2100		3575.3255(12)	27 961.499	3575.3255(12)	0.0000	$5s^26p$	$^2P^\circ_{3/2}$	$5s^27d$	$^2D_{5/2}$	72 377.4484	100 338.947	5.0+7	D+	Brill	TW
440		3582.3511(14)	27 906.663	3582.3511(13)	0.0000	$5s^26p$	$^2P^\circ_{3/2}$	$5s^27d$	$^2D_{3/2}$	72 377.4484	100 284.111	8.3+6	D+	Brill	TW
110		3612.68(22)	27 672.4	3612.71(3)	−0.03	$5s^27s$	$^2S_{1/2}$	$5s5p(^3P^\circ)6s$	$^2P^\circ_{1/2}$	86 280.318	113 952.44			Wu*	
240		3619.96(13)	27 616.7	3619.7860(12)	0.17	$5s^25d$	$^2D_{5/2}$	$5s^25f$	$^2F^\circ_{5/2}$	72 048.260	99 666.327	6.2+6	D	MS	AM
530		3620.4854(15)	27 612.732	3620.4872(10)	−0.0018	$5s^25d$	$^2D_{5/2}$	$5s^25f$	$^2F^\circ_{7/2}$	72 048.260	99 660.978	2.0+6	E	Brill	M79
500		3715.1524(11)	26 909.141	3715.1527(9)	−0.0003	$5s^26p$	$^2P^\circ_{1/2}$	$5s^28s$	$^2S_{1/2}$	71 493.273	98 402.412	1.6+7	D+	Brill	TW
440		3841.3756(14)	26 024.959	3841.3749(9)	0.0007	$5s^26p$	$^2P^\circ_{3/2}$	$5s^28s$	$^2S_{1/2}$	72 377.4484	98 402.412	2.9+7	D+	Brill	TW
190	*	3984.6(4)	25 089.8	3984.5(4)		$5s^24f$	$^2F^\circ_{7/2}$	$5s^211g$	$^2G_{9/2}$	89 288.255	114 378.1	2.4+6	D+	MS	TW
190	*	3984.6(4)	25 089.8	3984.5(4)		$5s^24f$	$^2F^\circ_{7/2}$	$5s^211g$	$^2G_{7/2}$	89 288.255	114 378.1	8.+4	E	MS	TW
17		3994.3(4)	25 028.7	3994.239(3)	0.0	$5s5p^2$	$^4P_{1/2}$	$5s^26p$	$^2P^\circ_{1/2}$	46 464.290	71 493.273			MS	
180	*	4110.3(4)	24 322.6	4110.3(3)	0.0	$5s^24f$	$^2F^\circ_{7/2}$	$5s^210g$	$^2G_{9/2}$	89 288.255	113 610.5	3.4+6	D+	MS	TW
180	*	4110.3(4)	24 322.6	4110.3(3)	0.0	$5s^24f$	$^2F^\circ_{7/2}$	$5s^210g$	$^2G_{7/2}$	89 288.255	113 610.5	1.2+5	E	MS	TW
180		4111.3(4)	24 316.2	4111.3(3)	0.0	$5s^24f$	$^2F^\circ_{5/2}$	$5s^210g$	$^2G_{7/2}$	89 294.055	113 610.5	3.3+6	D+	MS	TW
28		4164.8(3)	24 004.0	4164.76(4)	0.0	$5s^26d$	$^2D_{3/2}$	$5s5p(^3P^\circ)6s$	$^4P^\circ_{5/2}$	90 241.554	114 245.75			Wu	
31		4172.2(3)	23 961.4	4172.18(3)	0.0	$5s^27d$	$^2D_{3/2}$	$5s5p(^3P^\circ)5d$	$^4P^\circ_{3/2}$	100 284.111	124 245.66			Wu	
36	bl(Sn IV)	4216.2(6)	23 711	4216.28(4)	−0.1	$5s^26d$	$^2D_{3/2}$	$5s5p(^3P^\circ)6s$	$^2P^\circ_{1/2}$	90 241.554	113 952.44			Wu*	
170	*	4293.3(4)	23 285.6	4293.27(14)	0.0	$5s^24f$	$^2F^\circ_{7/2}$	$5s^29g$	$^2G_{9/2}$	89 288.255	112 574.0	5.1+6	D+	MS	TW
170	*	4293.3(4)	23 285.6	4293.27(14)	0.0	$5s^24f$	$^2F^\circ_{7/2}$	$5s^29g$	$^2G_{7/2}$	89 288.255	112 574.0	1.8+5	E	MS	TW
340		4294.33(15)	23 280.0	4294.33(14)	−0.00	$5s^24f$	$^2F^\circ_{5/2}$	$5s^29g$	$^2G_{7/2}$	89 294.055	112 574.0	4.9+6	D+	MS	TW
6		4323.0925(13)	23 125.086	4323.0922(13)	0.0003	$5s5p^2$	$^4P_{3/2}$	$5s^26p$	$^2P^\circ_{1/2}$	48 368.185	71 493.273	7.0+4	D+	Brill	OH10
120		4573.7(4)	21 858.0	4574.32(23)	−0.6	$5s^24f$	$^2F^\circ_{7/2}$	$5s^210d$	$^2D_{5/2}$	89 288.255	111 143.3			Wu	
91		4575.0(4)	21 851.8	4575.53(23)	−0.5	$5s^24f$	$^2F^\circ_{5/2}$	$5s^210d$	$^2D_{5/2}$	89 294.055	111 143.3			Wu	
	m			4579.9(3)		$5s^24f$	$^2F^\circ_{5/2}$	$5s^210d$	$^2D_{3/2}$	89 294.055	111 122.6			Wu	
150	*	4579.06(13)	21 832.4	4579.03(9)	0.03	$5s^24f$	$^2F^\circ_{7/2}$	$5s^28g$	$^2G_{9/2}$	89 288.255	111 120.8	8.0+6	D+	MS	TW
150	*	4579.06(13)	21 832.4	4579.03(9)	0.03	$5s^24f$	$^2F^\circ_{7/2}$	$5s^28g$	$^2G_{7/2}$	89 288.255	111 120.8	2.9+5	E	MS	TW
140		4580.22(13)	21 826.9	4580.25(9)	−0.03	$5s^24f$	$^2F^\circ_{5/2}$	$5s^28g$	$^2G_{7/2}$	89 294.055	111 120.8	7.7+6	D+	MS	TW
90		4618.2359(10)	21 647.226	4618.2363(10)	−0.0004	$5s5p^2$	$^4P_{5/2}$	$5s^26p$	$^2P^\circ_{3/2}$	50 730.224	72 377.4484	6.4+5	C+	Brill	OH10
48		4776.1(4)	20 931.7	4775.98(10)	0.1	$5s5p^2$	$^2P_{1/2}$	$5s^28p$	$^2P^\circ_{3/2}$	80 455.1	101 387.37			Wu	
62	h	4792.0732(19)	20 861.963	4792.0730(15)	0.0002	$5s^25d$	$^2D_{3/2}$	$5s^27p$	$^2P^\circ_{3/2}$	71 406.142	92 268.106	4.0+5	C+	Brill	OH10
100		4877.209(3)	20 497.805	4877.209(3)	0.000	$5s^25d$	$^2D_{3/2}$	$5s^27p$	$^2P^\circ_{1/2}$	71 406.142	91 903.945	5.6+6	B+	Brill	OH10

Table 1. (Continued.)

I_{obs} [a] arb. u.	Char. [b]	λ_{obs} [c] Å	σ_{obs} cm^{-1}	λ_{Ritz} [d] Å	$\delta\lambda_{O-Ritz}$ [e] Å	Classification				E_{low} cm^{-1}	E_{upp} cm^{-1}	A [f] s^{-1}		Acc [g]	Line Ref. [h]	TP Ref. [h]
66		4895.1(4)	20 422.9	4894.50(5)	0.6	$5s^26d$	$^2D_{5/2}$	$5s5p(^3P^\circ)6s$	$^4P^\circ_{3/2}$	90 351.894	110 777.28				Wu	
83		4917.1(4)	20 331.5	4917.8(3)	−0.7	$5s^27p$	$^2P^\circ_{3/2}$	$5s^211d$	$^2D_{5/2}$	92 268.106	112 596.9	3.4+6		D+	Wu	TW
150		4944.2562(20)	20 219.846	4944.2561(16)	0.0001	$5s^25d$	$^2D_{5/2}$	$5s^27p$	$^2P^\circ_{3/2}$	72 048.260	92 268.106	4.9+6		B+	Brill	OH10
360	*	5071.09(15)	19 714.1	5071.11(11)	−0.02	$5s^24f$	$^2F^\circ_{7/2}$	$5s^27g$	$^2G_{9/2}$	89 288.255	109 002.3	1.4+7		D+	MS	TW
360	*	5071.09(15)	19 714.1	5071.11(11)	−0.02	$5s^24f$	$^2F^\circ_{7/2}$	$5s^27g$	$^2G_{7/2}$	89 288.255	109 002.3	5.+5		E	MS	TW
	m			5071.63(11)		$5s^24f$	$^2F^\circ_{5/2}$	$5s^29d$	$^2D_{3/2}$	89 294.055	109 006.1				Wu	
360		5072.62(15)	19 708.2	5072.60(11)	0.02	$5s^24f$	$^2F^\circ_{5/2}$	$5s^27g$	$^2G_{7/2}$	89 294.055	109 002.3	1.3+7		D+	MS	TW
1600		5332.3391(16)	18 748.281	5332.3391(11)	0.0000	$5s^26p$	$^2P^\circ_{1/2}$	$5s^26d$	$^2D_{3/2}$	71 493.273	90 241.554	9.9+7		B+	Brill	OH10
2700		5561.9101(16)	17 974.443	5561.9094(15)	0.0007	$5s^26p$	$^2P^\circ_{3/2}$	$5s^26d$	$^2D_{5/2}$	72 377.4484	90 351.894	1.13+8		B+	Brill	OH10
2600		5588.8152(18)	17 887.913	5588.8153(16)	−0.0001	$5s^25d$	$^2D_{3/2}$	$5s^24f$	$^2F^\circ_{5/2}$	71 406.142	89 294.055	7.8+7		B+	Brill	OH10
530	h	5596.2644(15)	17 864.103	5596.2636(12)	0.0008	$5s^26p$	$^2P^\circ_{3/2}$	$5s^26d$	$^2D_{3/2}$	72 377.4484	90 241.554	1.91+7		B+	Brill	OH10
490		5796.9078(15)	17 245.794	5796.9075(13)	0.0003	$5s^25d$	$^2D_{5/2}$	$5s^24f$	$^2F^\circ_{5/2}$	72 048.260	89 294.055	5.1+6		B+	Brill	OH10
2700		5798.860(3)	17 239.988	5798.8578(18)	0.002	$5s^25d$	$^2D_{5/2}$	$5s^24f$	$^2F^\circ_{7/2}$	72 048.260	89 288.255	7.7+7		B+	Brill	OH10
470	H	5965.84(6)	16 757.46	5965.78(5)	0.06	$5s^27p$	$^2P^\circ_{3/2}$	$5s^29d$	$^2D_{5/2}$	92 268.106	109 025.72	7.6+6		D+	Brill	TW
1500	*	6077.6331(19)	16 449.220	6077.6304(16)	0.0027	$5s^24f$	$^2F^\circ_{7/2}$	$5s^26g$	$^2G_{9/2}$	89 288.255	105 737.482	2.7+7		D+	Brill	TW
1500	*	6077.6331(19)	16 449.220	6077.6304(16)	0.0027	$5s^24f$	$^2F^\circ_{7/2}$	$5s^26g$	$^2G_{7/2}$	89 288.255	105 737.482	1.0+6		D+	Brill	TW
1400		6079.7696(24)	16 443.439	6079.7742(18)	−0.0046	$5s^24f$	$^2F^\circ_{5/2}$	$5s^26g$	$^2G_{7/2}$	89 294.055	105 737.482	2.6+7		D+	Brill	TW
380		6242.1(7)	16 015.8	6241.13(15)	1.0	$5s^26d$	$^2D_{5/2}$	$5s^29p$	$^2P^\circ_{3/2}$	90 351.894	106 370.2				Wu	
760		6428.4(7)	15 551.7	6429.08(10)	−0.7	$5s^28s$	$^2S_{1/2}$	$5s5p(^3P^\circ)6s$	$^2P^\circ_{1/2}$	98 402.412	113 952.44				Wu*	
2500		6453.5422(12)	15 491.085	6453.5421(11)	0.0001	$5s^26s$	$^2S_{1/2}$	$5s^26p$	$^2P^\circ_{3/2}$	56 886.363	72 377.4484	7.0+7		B+	Brill	OH10
830		6569.7(7)	15 217.2	6568.51(11)	1.2	$5s^29d$	$^2D_{5/2}$	$5s5p(^3P^\circ)5d$	$^4P^\circ_{3/2}$	109 025.72	124 245.66				Wu	
1000		6661.1(8)	15 008.4	6661.1(8)		$5s^26d$	$^2D_{5/2}$	$5s^26f$	$^2F^\circ_{7/2}$	90 351.894	105 360.3	1.6+7		D+	Wu	TW
840		6760.812(3)	14 787.041	6760.8103(22)	0.002	$5s^26p$	$^2P^\circ_{1/2}$	$5s^27s$	$^2S_{1/2}$	71 493.273	862 80.318	3.82+7		B+	Brill	OH10
1300		6844.1859(20)	14 606.911	6844.1864(15)	−0.0005	$5s^26s$	$^2S_{1/2}$	$5s^26p$	$^2P^\circ_{1/2}$	56 886.363	71 493.273	6.0+7		B+	Brill	OH10
1100		7190.776(3)	13 902.873	7190.7778(24)	−0.002	$5s^26p$	$^2P^\circ_{3/2}$	$5s^27s$	$^2S_{1/2}$	72 377.4484	86 280.318	7.2+7		B+	Brill	OH10
670		7230.1(9)	13 827.3	7230.05(16)	0.1	$5s^27p$	$^2P^\circ_{1/2}$	$5s^28d$	$^2D_{3/2}$	91 903.945	105 731.3	1.2+7		D+	Wu	TW
500		7314.5(9)	13 667.7	7314.17(12)	0.3	$5s^27d$	$^2D_{3/2}$	$5s5p(^3P^\circ)6s$	$^2P^\circ_{1/2}$	100 284.111	113 952.44				Wu*	
480		7387.1651(24)	13 533.265	7387.1637(19)	0.0014	$5s5p^2$	$^2D_{3/2}$	$5s^26p$	$^2P^\circ_{3/2}$	58 844.181	72 377.4484	2.27+6		B+	Brill	OH10
380		7408.22(21)	13 494.8	7408.27(13)	−0.05	$5s^27p$	$^2P^\circ_{3/2}$	$5s^28d$	$^2D_{5/2}$	92 268.106	105 762.82	1.3+7		D+	MS	TW
450		7729.6(10)	12 933.7	7728.3(7)	1.3	$5s^25f$	$^2F^\circ_{7/2}$	$5s^211d$	$^2D_{5/2}$	99 660.978	112 596.9				Wu	
500		7741.425(3)	12 913.965	7741.423(3)	0.002	$5s5p^2$	$^2D_{5/2}$	$5s^26p$	$^2P^\circ_{3/2}$	59 463.481	72 377.4484	1.89+7		B+	Brill	OH10
	m			7745.1(3)		$5s^25f$	$^2F^\circ_{5/2}$	$5s^211d$	$^2D_{3/2}$	99 666.327	112 574.1				Wu	
190		7825.97(9)	12 774.45	7825.96(6)	0.01	$5s^27p$	$^2P^\circ_{1/2}$	$5s^29s$	$^2S_{1/2}$	91 903.945	104 678.41	4.7+6		D+	Brill	TW
280		7903.532(4)	12 649.091	7903.532(3)	0.000	$5s5p^2$	$^2D_{3/2}$	$5s^26p$	$^2P^\circ_{1/2}$	58 844.181	71 493.273	1.96+7		B+	Brill	OH10
53		8055.72(9)	12 410.13	8055.61(6)	0.11	$5s^27p$	$^2P^\circ_{3/2}$	$5s^29s$	$^2S_{1/2}$	92 268.106	104 678.41	8.6+6		D+	Brill	TW
2600	*	9058.880(4)	11 035.863	9058.886(3)	−0.006	$5s^24f$	$^2F^\circ_{7/2}$	$5s^25g$	$^2G_{9/2}$	89 288.255	100 324.111	6.8+7		D+	Brill	TW
2600	*	9058.880(4)	11 035.863	9058.886(3)	−0.006	$5s^24f$	$^2F^\circ_{7/2}$	$5s^25g$	$^2G_{7/2}$	89 288.255	100 324.111	2.4+6		D+	Brill	TW
2200		9063.658(5)	11 030.045	9063.649(4)	0.009	$5s^24f$	$^2F^\circ_{5/2}$	$5s^25g$	$^2G_{7/2}$	89 294.055	100 324.111	6.5+7		D+	Brill	TW
1300		10 607.434(6)	94 24.768	10 607.429(6)	0.005	$5s^26d$	$^2D_{3/2}$	$5s^25f$	$^2F^\circ_{5/2}$	90 241.554	99 666.327	4.9+7		D+	Brill	TW
1200		10 739.257(6)	93 09.081	10 739.254(5)	0.003	$5s^26d$	$^2D_{5/2}$	$5s^25f$	$^2F^\circ_{7/2}$	90 351.894	99 660.978	5.1+7		D+	Brill	TW
				23 521.14(24)		$5s^25p$	$^2P^\circ_{1/2}$	$5s^25p$	$^2P^\circ_{3/2}$	0.00	4251.494	6.94−1	M1	A+		B95

[a] Observed relative intensities, in terms of total energy flux under the line profile, are reduced to a common arbitrary scale corresponding to a plasma in local thermodynamic equilibrium with an effective excitation temperature of 4.2 eV. These conditions correspond to exposure 1 of the experiment of Wu [11] (see section 4.4).

[b] Character of observed line: bl—blended by a close line (the blending spectrum is indicated in parentheses); h—hazy line; H—very hazy line; s—asymmetric line extending towards shorter wavelengths; *—intensity shared by two or more transitions; m—masked by a stronger neighboring line (no wavelength measured); : —the wavelength was not measured (the value in λ_{obs} is a rounded Ritz wavelength).

[c] Observed and Ritz wavelengths are given in standard air for wavenumbers σ between 5000 cm^{-1} and 50 000 cm^{-1} and in vacuum outside of this range. The uncertainty (standard deviation) in the last digit is given in parentheses.

[d] Ritz wavelengths and their uncertainties were determined in the least-squares level optimization procedure (see section 4.3).

[e] Difference between observed and Ritz wavelength. If this column is blank, and λ_{obs} is not blank, this line alone determines one of the levels involved in the assigned transition. An 'x' after the value indicates that this line was excluded from the level optimization.

[f] In the transition probability values, the number after the '+' or '−' symbol means the power of 10.

[g] Transition probability accuracy code is explained in table 6.

[h] References to observed wavelengths and transition probabilities: AM—Alonso-Medina and Colón 2000 [48]; B95—Biémont *et al* 1995 [49]; Brill—Brill 1964 [11]; M79—Miller *et al* 1979 [53]; MS—McCormick and Sawyer 1938 [6]; OH10—Oliver and Hibbert 2010 [14]; Wu—Wu 1967 [11]; Wu*—line measured by Wu [11] with our new or revised classification; TW—this work.

for deriving accurate energy level values from the observed wavelengths. For that purpose, it is necessary to estimate the uncertainty for each individual line. The two main factors determining our measurement uncertainty are the uncertainties of the reference wavelengths and statistical uncertainties in measuring the line positions on the plates. The first of these two factors contributes to the systematic uncertainty. About 70% of the used reference wavelengths have uncertainties ⩽0.003 Å. However, in order to provide a sufficiently uniform coverage of the studied wavelength range, in some regions we had to use a few less accurately known wavelengths with uncertainties up to 0.005 Å. The uncertainties of the reference lines were either taken from the original papers or estimated from deviations of the quoted reference wavelengths from the Ritz values given in the ASD database [5]. Our statistical uncertainties greatly depend on the shape and width of the line profiles. The width (full width at half-maximum) of a selection of 23 lines on our plates in the region 1190–1800 Å was roughly estimated from the comparator displacement readings and the known dispersion factor. For isolated symmetrical lines showing no visible broadening, the widths were 0.02–0.04 Å, while several lines, appearing as hazy, showed a significant broadening of up to 0.15 Å. We attribute this clearly visible broadening to autoionization of the upper level. Statistical uncertainties of the measurement of line position on the plates, estimated by repeated measurements, were the greatest for the widest lines, which were those with longest wavelengths and those widened by autoionization. One of our plates had unusually large line widths in the long wavelength region, which was excluded from the measurements. Positions of sharp isolated lines could be measured on our comparator with uncertainties of about 2 μm for the shortest wavelengths and up to 5 μm for the longest ones. This corresponds to statistical uncertainties of about 0.003 Å at 900 Å and 0.007 Å at 1900 Å. For the widest lines broadened by autoionization, we estimated the statistical uncertainty by extrapolation, i.e., by multiplying the uncertainty of narrow lines in the same region by the ratio of the line widths, yielding uncertainties as large as 0.02 Å. For blended lines, the uncertainty was doubled. Most of the lines were measured on two to four plates, and some were also measured in the second order of diffraction. For such multiply measured lines the statistical uncertainty of the reported average wavelength was significantly reduced, leaving the uncertainty of the reference lines as the main contributing factor. The values of uncertainty assigned to each line can be found in table 1. They vary from 0.006 Å for sharp lines below 1050 Å to 0.02 Å for very wide and blended lines. All uncertainties reported in the present work are meant to be on the level of one standard deviation.

Many of the known classified lines of Sn II were observed by other researchers [6, 10, 11] outside the wavelength range studied in the present work. Thus, to obtain optimized level values, wavelength values and uncertainties reported by other observers have to be evaluated.

The most valuable of the previously reported measurements are those of Brill [10] made with an electrodeless discharge tube as a light source. He reported 42 wavelengths of Sn II between 2150 Å and 10 740 Å, with uncertainties estimated individually for each line. For 39 of these lines, the measurements were made with a Fabry–Perot interferometer, and their uncertainties vary between 0.0006 Å and 0.006 Å. Three weak lines were measured with a 9.14 m, 590 lines mm^{-1} grating spectrograph having inverse linear dispersion of 1.7 Å mm^{-1}. Uncertainties of these three lines are between 0.06 Å and 0.09 Å, as reported by Brill [10].

Two other large sets of wavelengths were taken from Wu's thesis [11] and from McCormick and Sawyer [6]. Wu photographed the tin spectra in the region between 350 Å and 9000 Å using an electrodeless discharge. A condensed spark in helium with a 3 m normal incidence vacuum grating spectrograph and a prism spectrograph were used in the regions below and above 2400 Å, respectively. Wu reported a total of 3403 spectral lines, of which he assigned 110 to Sn I, 128 to Sn II, 321 to Sn III, 177 to Sn IV, and 118 to Sn V, leaving the remaining 2549 lines unassigned to a particular ionization stage. Although all wavelengths in Wu's line list were given with three digits after the decimal point (in angstroms), the wavelength uncertainty varied greatly depending on the wavelength region and on the spectrographs used.

To assess the uncertainties of Wu's wavelength measurements, we compared his reported wavelengths with more accurate Sn I measurements and with Sn II Ritz wavelengths. The reference wavelengths of Sn I were taken mainly from Brill's thesis [10] for wavelengths above 2064 Å and from absorption measurements of Brown *et al* [28] below that. Both sets have uncertainties less than 0.002 Å. The Sn II Ritz wavelengths (see section 4) were determined mainly by our measurements in the VUV and by Brill's measurements [10] in the air region.

The comparison shown in figures 1(a)–(c) revealed significant systematic shifts in Wu's measurements. These shifts vary smoothly with wavelength between +0.019 Å near 900 Å and −0.25 Å near 8300 Å. The presence of systematic shifts in the earlier measurements is not surprising, since the spectrometers used therein had poorer resolution. For example, the grating spectrograph used by Wu [11] was equipped with a 1200 lines mm^{-1} grating, in contrast to our 2400 lines mm^{-1} (although Wu did not specify what grating he used, we assume it was the same as described in Bhatia's thesis [29] made at the same institution two years later). Thus, our spectrometer had a twice greater resolving power. The grating used by McCormick and Sawyer [6] had only 567 lines per mm, and its radius of curvature was 1 m, three times less than in our spectrometer. Thus, in their work the reciprocal linear dispersion was 17 Å, more than an order of magnitude worse than in our work. The quality and number of available wavelength standards has also greatly improved since the work of Wu [11] and especially McCormick and Sawyer [6]. In particular, the high-precision measurements of Brill [10] in Sn I and Sn II were not available to those authors. Nevertheless, as often happens with old measurements, they can be re-calibrated using improved internal standards of the same spectrum. This re-calibration is done here by subtracting the systematic shifts shown in figure 1. After this subtraction, the measurement uncertainties of the corrected wavelengths were

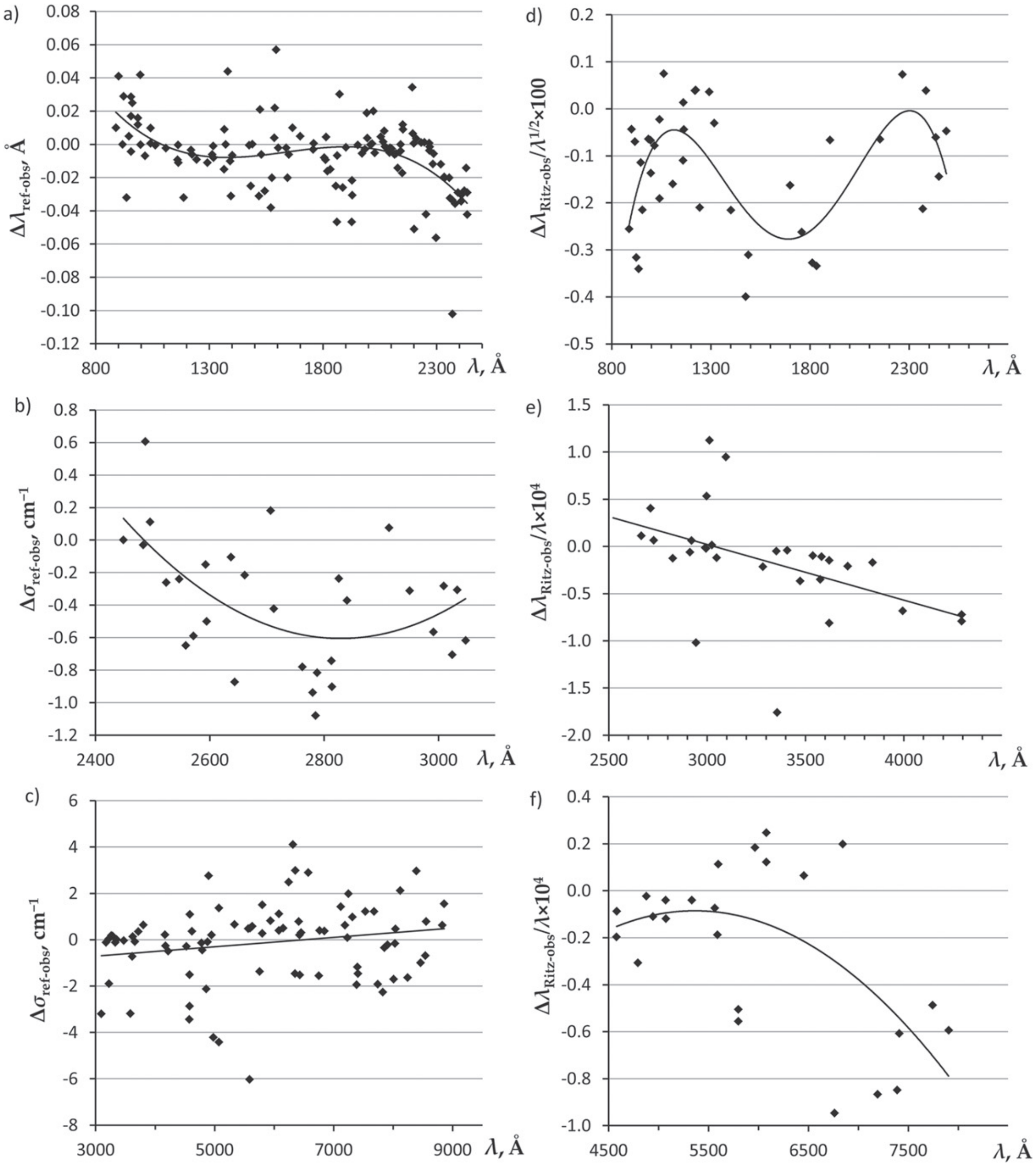

Figure 1. Differences between observed and reference wavelengths λ or wave numbers σ for the measurements of Wu [11] (a)–(c) and McCormick and Sawyer [6] (d)–(f). The solid lines are linear or polynomial fits determining the systematic corrections to the original measurements.

estimated from their average deviations from reference values. In the region below 2400 Å, where the grating spectrograph was used, the estimated wavelength uncertainty is almost constant, about 0.019 Å. In the region 2400 Å to 3050 Å, where the quartz prism spectrograph was used, the uncertainties are about 0.024 Å on average. However, uncertainties of Wu's prism spectra are better described by a constant uncertainty in wavenumber, about 0.3 cm^{-1} for this wavelength region. This implies a gradual increase of uncertainties from 0.019 Å at 2400 Å to 0.03 Å at 3050 Å. Above this wavelength, as figure 1(c) shows, uncertainties increase abruptly to 1.7 cm^{-1}, corresponding to 0.16 Å at 3100 Å and 1.2 Å at 8300 Å. We note that the plots in figure 1 use different scales on the vertical axes in order to make the random scatter of the data points nearly constant in magnitude throughout the wavelength ranges covered by the panels. Then the correction polynomial curves can be easily found by unweighted interpolation.

McCormick and Sawyer [6] excited the Sn II spectrum in a hollow cathode discharge in helium and photographed it in a similarly wide wavelength range from 800 Å to 10 000 Å. In the region below 2200 Å, they used a 1 m vacuum grating spectrograph. The region from 2200 Å to 2700 Å was photographed with a quartz prism spectrograph. Above 2700 Å, two other prism spectrographs were used. Since these authors reported only the Sn II wavelengths, the only means of assessment of their uncertainties was a comparison with more accurate Ritz wavelengths. For this comparison, we used the Ritz wavelengths from our preliminary level optimization (see section 4) that were mainly determined by our VUV measurements and those of Brill [10] in the region above 2150 Å. Figure 1(d) shows these deviations, scaled in such a way that their scatter has similar magnitudes throughout the wavelength range covered by the figure.

As with the work of Wu, measurements of McCormick and Sawyer [6] appear to have significant systematic shifts smoothly varying with wavelength, from −0.11 Å at 1700 Å to zero at 2300 Å. At longer wavelengths, as figures 1(e) and (f) show, statistical uncertainties appear to be almost constant, if they are scaled by dividing them by wavelength. Systematic shifts are significant in these regions as well, varying from +0.08 Å at about 3000 Å to 0.6 Å at 8000 Å.

All identified lines of Sn II are collected in table 1 with the adopted wavelengths and their uncertainties. In total, there are about 200 lines, of which 70 were measured in the present work, 42 are from Brill [10], 27 are from McCormick and Sawyer [6], and 63 are from Wu [11]. Among Wu's lines [11], 12 were classified as Sn II transitions by us.

4. Results and discussion

4.1. Theoretical calculations

The theoretical calculation for energy levels, wavelengths, and transition probabilities of Sn II was made with Cowan's codes [30], which implement the Hartree–Fock (HF) method with perturbative account for relativistic and configuration-interaction (CI) effects. For the even parity system, the configurations included were $5s5p^2$, $5s^2ns$ ($n=6$–12), $5s^2nd$ ($n=5$–12), $5s^2ng$ ($n=5$–12), 4f5s5p, and $5s5d^2$; the odd parity set included $5s^2np$ ($n=6$–20), $5s^2nf$ ($n=4$–20), $5p^3$, 5s5p5d, 5s5p6s, 4f5s5d, $4f5p^2$, and $5p5d^2$ configurations. The initial scaling of the Slater parameters was 100% of the HF values for E_{av} and ζ_{nl}, while the F^k, G^k, and the CI parameters were scaled to 80% of the HF values. Then the Slater parameters were varied in the least-squares fitting (LSF) procedure minimizing discrepancies between calculated and observed level values.

In the parametric fitting, the energy level calculations for even parity converged with a standard deviation of 77 cm^{-1}, while the odd-parity configurations were fitted with a standard deviation of 156 cm^{-1}. Transition probabilities and autoionization rates were calculated with wavefunctions modified according to the fitted parameters.

4.2. Analysis of the spectrum

4.2.1. The $5s^25p-(5s^2(ns+nd)+5s5p^2)$ transition array.

Excitation of the outer electron from the $5s^25p$ $^2P°$ ground term leads to the $5s^2ns$ $^2S_{1/2}$ and $5s^2nd$ $^2D_{3/2,5/2}$ level series showing a simple doublet structure. The transitions from $5s^2ns$ $^2S_{1/2}$ ($n=6$–8) to both levels of the ground term and those from $5s^29s$ to $5s^25p$ $^2P°_{3/2}$ were already reported by McCormick and Sawyer [6]. The energy levels derived from their wavelengths were later improved by Shenstone and reported in AEL [4]. All these transitions are confirmed in our measurements with improved accuracy. McCormick and Sawyer [6] established the levels of $5s^210s$ and 11s by observing transitions to the $5s^26p$ levels in the air wavelength region. We were able to observe both transitions from $5s^29s$ to the levels of $5s^25p$ at 955.299 Å ($^2S_{1/2}\rightarrow{}^2P°_{1/2}$) and 995.742 Å ($^2S_{1/2}\rightarrow{}^2P°_{3/2}$). Wu [11] observed both transitions from $5s^210s$ to the ground-term levels. Other transitions from $5s^2ns$ ($n=7$–11) to the $5s^2np$ ($n=6$–7) levels have also been observed by us and by other researchers [6, 10, 11]. Thus, the levels of the $5s^2ns$ ($n=6$–11) configurations are well established. They are almost unperturbed, showing the leading *LS* percentages of their composition above 99%. Consistent trends of our LSF parameter values along both *n*s and *n*d series and good agreement of observed and predicted relative line intensities confirm all their identifications.

The $5s^2nd$ configurations were also listed in AEL [4]. We confirmed the levels of $5s^2nd$ ($n=5$–9) with lines observed on our plates. Wu's identifications of transitions from the $5s^210d$ and 11d configurations [11] are also confirmed. Some additional transitions between the $5s^2np$ ($n=6$–8) and $5s^2nd$ levels have also been observed (see table 1). It is important to mention here that there is a strong interaction between the $5s^25d$ and $5s5p^2$ configurations. For this reason, the $^2D_{3/2,5/2}$ levels of these configurations are strongly mixed with each other. This strong mixing was indicated by relativistic CI calculations of Oliver and Hibbert [14], which, however, favored the old AEL designations. Percentage compositions of eigenvectors resulting from our calculations suggest that the configuration labels given in AEL for these two pairs of levels should be interchanged (see table 3). Nevertheless, to avoid confusion in line identifications we retained the AEL labels adopted also by Sansonetti and Martin [31].

Another type of excitation is represented by excitation of the inner 5s electron to the 5p shell, leading to the $5s5p^2$ configuration with seven levels containing a quartet and three doublet terms. All three quartet levels were firmly established by Brill [10], who observed four intercombination lines from these levels to the ground term $5s^25p$ $^2P°_{1/2,3/2}$. In the present work, we confirm two of the doublet levels including $^2P_{1/2}$ at 80 455.8 cm^{-1} reported in AEL [4] as questionable. We observed both transitions from this level to the ground term. However, we could not confirm the $^2S_{1/2}$ level reported at 80 206.1 cm^{-1}. This level value was questionable for two reasons. Firstly, it strongly deviated from the LSF calculations. Secondly, its strongest predicted transition to the ground level was missing in our spectra. In Wu's line list this level value is supported by two observed lines classified as transitions to the ground term, However, Wu's observed intensity for the line he interpreted as the $5s^25p$ $^2P°_{1/2}-5s5p^2$ $^2S_{1/2}$ transition with $\Delta J=0$ is four times smaller than for his classification of the $\Delta J=-1$ transition, while our calculation

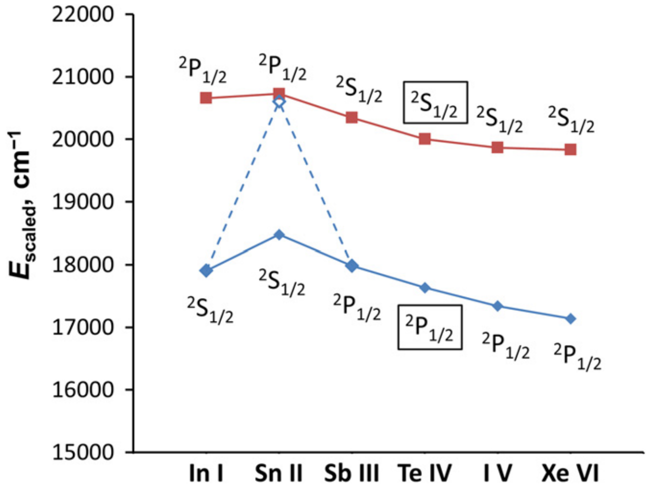

Figure 2. Isoelectronic comparison of scaled energies, $E_{scaled} = (E - 39\,000)/Z_c$, of the strongly mixed $5s5p^2$ $^2S_{1/2}$ and $^2P_{1/2}$ levels. The dominant term labels of the lower and upper levels interchange at ionic core charge $Z_c = 3$ (Sb III). The open circle just below the $^2P_{1/2}$ data point for Sn II indicates the previously adopted position of the $^2S_{1/2}$ level in Sn II at 80 206 cm^{-1} [4]. Dashed lines connecting this data point with the other ones of the lower level show how this graph would look if that incorrect value were used instead of our revised value (solid rhombs and lines). Solid boxes indicate the revised term labels for Te IV. See table 2 for details.

predicts it to be greater by a factor of 3×10^4. Therefore, this level value was rejected. We further disagree with the recent 'verification' of this level value by Alonso-Medina *et al* [17] based on one $5s5p^2$ $^2S_{1/2} - 5s5p(^3P°)6s$ $^4P°_{1/2}$ transition they presumably observed at 3418.9 Å (as shown in their figure 2). According to our calculations, this intercombination transition should be too weak to be observable. Its radiative rate is at least four orders of magnitude smaller than that of the two *LS*-allowed transitions from the same upper level to $5s5p^2$ $^4P_{1/2,3/2}$. Connerade and Baig [32] revised the identification of the $5s5p^2$ $^2P_{1/2}$ and $^2P_{3/2}$ levels by analyzing level separations along the In I isoelectronic sequence. Their suggested values for these two levels were 80 206 cm^{-1} and 81 718 cm^{-1}, respectively (i.e., they changed the term assignment of the value 80 206 cm^{-1} from $^2S_{1/2}$ to $^2P_{1/2}$ and retained Moore's questionable assignment of the $5s5p^2$ $^2P_{3/2}$ level). We confirmed the identification of the second level and refined its position. However, the first one, as noted above, was found to be spurious. Calculations of Connerade and Baig [32] yielded a predicted value for the $5s5p^2$ $^2S_{1/2}$ level at 60 024 cm^{-1}. We located this level at a much higher position, at 75 954.3 cm^{-1}, by identifying transitions from it to both levels of the ground term. The strongest of these transitions (to $^2P_{1/2}$) was observed in our spectra at 1316.572 Å. A line near this wavelength was previously interpreted by Wu [11] as the $5s^25p$ $^2P°_{3/2} - 5s5p^2$ $^2S_{1/2}$ transition. That $\Delta J = -1$ transition, predicted to be much weaker than $\Delta J = 0$, was not observed on our plates. However, it was observed by Wu [11] at 1394.667 Å as a relatively weak line in two exposures. The newly revised $5s5p^2$ $^2S_{1/2}$ level value fits well in our parametric LSF calculations with reasonable values of the fitted parameters. This identification is further validated by an isoelectronic comparison presented in figure 2 for the sequence In I to Xe VI. The $^2S_{1/2}$ and $^2P_{1/2}$ levels of $5s5p^2$ are strongly mixed in these spectra. In In I, the leading terms are ^2S and ^2P for the lower and upper of these two levels, respectively, while in Xe VI they are reversed. The previously adopted position of $5s5p^2$ $^2S_{1/2}$ level in Sn II, indicated by dashed lines in figure 2, is strikingly inconsistent with the smooth isoelectronic trend of other data points. Our new LSF calculations for this sequence result in interchange of the term labels $^2S_{1/2}$ and $^2P_{1/2}$ in Te IV and predict a much lower position for the $^2S_{1/2}$ level in Sn II. This prediction is in qualitative agreement with findings of Connerade and Baig [32]. As indicated by the solid lines in figure 2, our revised identification produces a smooth isoelectronic trend for the lower $J = 1/2$ level, similar to the behavior of the upper level. The revised level values and term labels, along with the calculated percentage compositions, are given in table 2. Additional support for our new identification of the $5s5p^2$ $^2S_{1/2}$ level in Sn II is provided by a recent theoretical calculation by Oliver and Hibbert [14]. They predicted $^2S_{1/2}$ in Sn II to be at 76 215 cm^{-1}, which is in close agreement with our newly found level value. Colón and Alonso-Medina [33] suggested an explanation of the anomaly in the $5s5p^2$ $^2S_{1/2}$ and $^2P_{1/2}$ levels of Sn II by the presence of some mysterious interacting configuration(s). As this anomaly is now resolved, their suggestion can be dismissed. It should be noted that these two levels are strongly mixed (see tables 2 and 3). Thus, their *LS* labels have little physical meaning and are used in our tables for bookkeeping purpose only.

4.2.2. The $5p^3$ and $5s5p(5d+6s)$ configurations. These configurations arise from excitation of the $5s5p^2$ configuration. In the sequence Sb III—I V [37–39], transitions from these configurations have been observed in the Antigonish laboratory with moderate intensity. Therefore, we expected them to occur in Sn II as well. Our preliminary calculations for Sn II show that these configurations strongly interact with each other and also with other configurations, e.g., 4f5s5d and $5p5d^2$, which are completely unknown at present. The $5p^3$ and $5s5p(5d+6s)$ configurations are predicted to extend past the ionization limit. Thus, many of their levels should be autoionizing, making the analysis more difficult. Additional complication stems from the fact that some of the levels of these configurations are embedded within highly excited levels of the $5s^2np$ and nf series, with which they strongly interact. A few levels of these configurations were listed in AEL [4] with incomplete designations; some were marked as doubtful. We attempted to improve interpretation of these levels. The level at 109 223.4 cm^{-1} in AEL [4] is supported by two transitions terminating on the $5s5p^2$ $^4P_{1/2,3/2}$ levels, observed in our spectra, and one transition to $5s^25d$ $^2D_{3/2}$ observed by Wu [11]. We now identified this level as $5s^210p$ $^2P_{1/2}$ on the basis of our LSF calculation. Observed relative intensities of the lines are in satisfactory agreement with calculations. We were able to confirm the quartet levels of 5s5p6s configuration listed in AEL [4], as they give rise to strong transitions to the lowest quartet levels of the $5s5p^2$ configuration. The level at

Table 2. The two $J = 1/2$ doublet levels of the 5s5p^2 configuration in the In I isoelectronic sequence. All percentage compositions and the Sn II energies are from the present work; for the rest of the data the references are given in the first column.

Isoelectronic member	Lower level				Upper level			
	Energy, (cm^{-1})	Percentages ^{2}S	^{2}P	Term label	Energy, (cm^{-1})	Percentage ^{2}S	^{2}P	Term label
In I [34]	56 906	74	24	^{2}S	59 657	23	76	^{2}P
Sn II	75 954.3[a]	51	46	^{2}S	80 455.1	45	53	^{2}P
Sb III [4]	92 948.9	31	37	^{2}P[b]	100 010	57	41	^{2}S
Te IV [4]	109 536	40	57	^{2}P[c]	119 009	56	42	^{2}S[c]
I V [35]	125 703.5	36	61	^{2}P	138 328.3	60	38	^{2}S
Xe VI [36]	141 837.2	32	64	^{2}P	157 995.6	62	36	^{2}S

[a] Our revised value replaces the previously reported 80 206 cm^{-1} [4].
[b] Third leading component: 31% of 5s^{2}6s ^{2}S (at 93 417.8 cm^{-1} [4]).
[c] The level designations for Te IV are interchanged according to our LSF calculations.

113 819.0 cm^{-1} is also confirmed. In AEL [4], the J value of this level was given as 3/2 with a question mark, and no configuration label was attributed to it. Our present calculation with extensive configuration interaction shows that this level should be assigned to ^{2}D$_{5/2}$ of the 5s5p5d configuration.

As noted above, identification of autoionizing levels presented considerable difficulties. We could not confirm the level at 124 627.7 cm^{-1} in AEL [4]. Wu [11] assigned three observed lines at 1520.153 Å, 2907.33 Å, and 7412.5 Å to this level. However, no satisfactory match could be found for this level in our calculations. All other autoionizing levels given in AEL [4] have been identified in our spectra. In particular, three levels previously reported at 123 156, 132 168 and 132 708 cm^{-1} with uncertain designations are found to be associated with the 5p^3 configuration. The first of them is identified as 5p^3 ^{4}S°$_{3/2}$, while the other two have dominant contributions of 5s5p(^{1}P°)5d ^{2}D°$_{3/2}$ and ^{2}D°$_{5/2}$, respectively. Since the 5s5p5d configuration strongly interacts with 5p^3, these levels have large admixtures of 5p^3 ^{2}D° in their wavefunctions. A few of the other autoionizing levels that were based on just one or two observed transitions remain questionable. In all such cases, the observed lines attributed to these levels are the strongest predicted ones.

4.2.3. The 5s^{2}np and 5s^{2}nf configurations. After the successful establishment of the 5s^2ns and nd levels, a further analysis of the 5s^2np and nf configurations was undertaken. The 5s^2np ($n = 6$–9) and 5s^2nf ($n = 4$–6) configurations were already reported in AEL [4]. Some transitions from 5s^{2}6p and 7p to levels of the 5s^{2}6s, 5s^{2}5d, and 5s5p^2 configurations were measured interferometrically by Brill [10]. Lines arising from the 5s^2np ($n = 6$–9) configurations were classified by McCormick and Sawyer [6], and some additional lines were also observed by Wu [11]. We confirm all these identifications, as the observed level energies and relative line intensities are in satisfactory agreement with our calculations.

The 5s^{2}6f ^{2}F°$_{7/2}$ level was given by Moore [4] at 105 367 cm^{-1}, while the $J = 5/2$ level of this configuration was previously unknown. On our plates, we did not observe any transitions from the $J = 7/2$ level. In Wu's line list [11], the only line placing this level near the AEL value is at 6661.1 Å, which we tentatively interpreted as the 5s^{2}6d ^{2}D$_{5/2}$ – 5s^{2}6f ^{2}F°$_{7/2}$ transition. This interpretation yields the position of the $J = 7/2$ level at 105 360.3 cm^{-1}, slightly lower than the AEL value. However, this transition is by far not the strongest predicted from this level. The 5s^{2}5d ^{2}D$_{5/2}$ – 5s^{2}6f ^{2}F°$_{7/2}$ transition, predicted to occur at 2178.12 Å, should be about ten times stronger, but there is no line near this wavelength in Wu's list [11]. Another possible transition to the 5s5p^2 ^{4}P$_{5/2}$ level should occur at 1830.49 Å with approximately the same intensity as 5s^{2}6d ^{2}D$_{5/2}$ – 5s^{2}6f ^{2}F°$_{7/2}$. Neither our plates nor Wu's line list show a line near this wavelength. Thus, we retained the above tentative identification with a question mark. In the search for the missing 5s^{2}6f ^{2}F°$_{5/2}$ level, we relied on the expectation that the $J = 5/2$–7/2 fine-structure interval should be slightly greater than the value predicted by our LSF, 3 cm^{-1}. This expectation was grounded on the observation that experimental values for this interval in the 5s^{2}4f and 5s^{2}5f configurations, 5.800(5) cm^{-1} and 5.349 (8) cm^{-1}, are close to the LSF values, 3.7 cm^{-1} and 3.4 cm^{-1}, respectively. The only suitable pair of observed lines was found at 2148.61 Å (from McCormick and Sawyer [6]) and 2943.30 Å (from Wu [11]). We tentatively classified these lines as transitions from 5s^{2}6f ^{2}F°$_{5/2}$ to the 5s^{2}5d ^{2}D$_{3/2}$ and 5s5p^2 ^{2}D$_{3/2}$ levels, respectively. Wu has a line 2148.85 Å identified as a Sn III transition, which could possibly mask the first of these two lines. However, the second line at 2943.30 Å, as observed by Wu [11], is a factor of ten stronger than expected from our predicted intensities (see section 4.4), while several other transitions from the same level, predicted to be stronger or of comparable intensities, were not observed. Furthermore, the $J = 5/2$–7/2 fine-structure interval 11.4(18) cm^{-1} resulting from the above classifications appears to be greater than expected. Thus, both our values for the 5s^{2}6f ^{2}F°$_{5/2}$ and 5s^{2}6f ^{2}F°$_{7/2}$ levels are questionable and need further confirmation.

4.2.4. Levels of 5s^{2}ng configurations. The 5s^2ng ($n = 6$–11) ^{2}G energy levels were established by transitions from the levels of 5s^{2}4f configuration, identified primarily by

Table 3. Optimized energy levels of Sn II.

Configuration	Term	*J*	Energy[a] (cm^{-1})		Unc.[b] (cm^{-1})	Leading percentages[c]				ΔE_{o-c}[d] (cm^{-1})	No. of lines[e]
$5s^25p$	$^2P^\circ$	1/2	0.00		0.05	97	2	$5p^3$	$^2P^\circ$	81	17
$5s^25p$	$^2P^\circ$	3/2	4251.494		0.014	97	2	$5p^3$	$^2P^\circ$	−81	25
$5s5p^2$	^4P	1/2	46 464.290		0.018	98				−63	12
$5s5p^2$	^4P	3/2	48 368.185		0.007	99				−20	17
$5s5p^2$	^4P	5/2	50 730.224		0.005	97	3	$5s5p^2$	^2D	80	12
$5s^26s$	^2S	1/2	56 886.363		0.003	100				0	7
$5s5p^2$	^2D	3/2	58 844.181		0.004	41	58	$5s^25d$	^2D	−128	17
$5s5p^2$	^2D	5/2	59 463.481		0.005	38	59	$5s^25d$	^2D	128	12
$5s^25d$	^2D	3/2	71 406.142		0.008	41	54	$5s5p^2$	^2D	−120	11
$5s^26p$	$^2P^\circ$	1/2	71 493.273		0.003	99				3	14
$5s^25d$	^2D	5/2	72 048.260		0.007	40	56	$5s5p^2$	^2D	119	12
$5s^26p$	$^2P^\circ$	3/2	72 377.4484			99				−3	16
$5s5p^2$	^2S	1/2	75 954.3	R	0.4	51	46	$5s5p^2$	^2P	105	3
$5s5p^2$	^2P	1/2	80 455.1	C	0.4	53	45	$5s5p^2$	^2s	−120	3
$5s5p^2$	^2P	3/2	81 718.3		0.3	97	2	$5s5p^2$	^2D	18	3
$5s^27s$	^2S	1/2	86 280.318		0.005	99				0	5
$5s^24f$	$^2F^\circ$	7/2	89 288.255		0.007	96	3	$4f5p^2$	$^2F^\circ$	−1	10
$5s^24f$	$^2F^\circ$	5/2	89 294.055		0.006	96	3	$4f5p^2$	$^2F^\circ$	1	11
$5s^26d$	^2D	3/2	90 241.554		0.004	97	2	$5s5p^2$	^2D	−27	7
$5s^26d$	^2D	5/2	90 351.894		0.005	97	2	$5s5p^2$	^2D	26	6
$5s^27p$	$^2P^\circ$	1/2	91 903.945		0.015	99				−2	6
$5s^27p$	$^2P^\circ$	3/2	92 268.106		0.009	99				2	10
$5s^28s$	^2S	1/2	98 402.412		0.006	100				0	5
$5s^25f$	$^2F^\circ$	7/2	99 660.978		0.006	99				−1	4
$5s^25f$	$^2F^\circ$	5/2	99 666.327		0.006	99				1	4
$5s^27d$	^2D	3/2	100 284.111		0.010	99				−11	6
$5s^25g$	^2G	7/2	100 324.111	C	0.007	100				0	2
$5s^25g$	^2G	9/2	100 324.111	C	0.007	100				0	1
$5s^27d$	^2D	5/2	100 338.947		0.009	99				11	2
$5s^28p$	$^2P^\circ$	1/2	101 204.2		0.4	99				4	2
$5s^28p$	$^2P^\circ$	3/2	101 387.37		0.16	99				1	5
$5s^29s$	^2S	1/2	104 678.41		0.10	100				0	6
$5s^26f$	$^2F^\circ$	7/2	105 360.3	?	1.8	99				9	1
$5s^26f$	$^2F^\circ$	5/2	105 371.7	N?	0.3	99				17	2
$5s^28d$	^2D	3/2	105 731.3		0.3	100				−6	5
$5s^26g$	^2G	7/2	105 737.482		0.007	100				0	2
$5s^26g$	^2G	9/2	105 737.482		0.007	100				0	1
$5s^28d$	^2D	5/2	105 762.82		0.23	100				6	3
$5s^29p$	$^2P^\circ$	1/2	106 256.4	N	0.3	99				−28	2
$5s^29p$	$^2P^\circ$	3/2	106 370.2		0.4	99				−26	3
$5s^210s$	^2S	1/2	108 357.6		0.4	100				0	4
$5s^27g$	^2G	7/2	109 002.3		0.4	100				0	2
$5s^27g$	^2G	9/2	109 002.3		0.4	100				0	1
$5s^29d$	^2D	3/2	109 006.1		0.4	100				−4	3
$5s^29d$	^2D	5/2	109 025.72		0.15	100				4	4
$5s^210p$	$^2P^\circ$	1/2	109 222.6	R	0.3	81	16	$5s5p(^3P^\circ)6s$	$^4P^\circ$	61	3
$5s5p(^3P^\circ)6s$	$^4P^\circ$	1/2	109 453.6		0.3	81	18	$5s^210p$	$^2P^\circ$	−13	2
$5s^211s$	^2S	1/2	110 699		4	100				1	1
$5s5p(^3P^\circ)6s$	$^4P^\circ$	3/2	110 777.28		0.21	79	12	$5s^211p$	$^2P^\circ$	−11	5
$5s^28g$	^2G	7/2	111 120.8		0.4	100				0	2
$5s^28g$	^2G	9/2	111 120.8		0.4	100				0	1
$5s^210d$	^2D	3/2	111 122.6		1.2	100				−7	2
$5s^210d$	^2D	5/2	111 143.3		1.1	100				5	4
$5s^29g$	^2G	7/2	112 574.0		0.8	100				0	2
$5s^29g$	^2G	9/2	112 574.0		0.8	100				0	1
$5s^211d$	^2D	3/2	112 574.1	N	0.5	100				−8	2
$5s^211d$	^2D	5/2	112 596.9		1.1	100				9	3
$5s^210g$	^2G	7/2	113 610.5		1.5	100				0	2

Table 3. (Continued.)

Configuration	Term	J	Energy[a] (cm^{-1})		Unc.[b] (cm^{-1})	Leading percentages[c]				ΔE_{o-c}[d] (cm^{-1})	No. of lines[e]
$5s^2 10g$	^2G	9/2	113 610.5		1.5	100				0	1
$5s5p(^3P°)5d$	$^2D°$	5/2	113 818.65	R	0.21	62	18	$5p^3$	$^2D°$	44	4
$5s5p(^3P°)6s$	$^2P°$	1/2	113 952.44	N	0.23	30	50	$5s^2 14p$	$^2P°$	9	6
$5s5p(^3P°)6s$	$^4P°$	5/2	114 245.75		0.20	95	2	$5s5p(^3P°)5d$	$^2D°$	9	6
$5s^2 11g$	^2G	7/2,9/2	114 378.1		2.2	100				0	1
$5s5p(^3P°)5d$	$^4F°$	5/2	115 256.2	N?	0.3	76	8	$5s5p(^3P°)5d$	$^2D°$	−31	1
$5s5p(^3P°)5d$	$^4F°$	7/2	116 423.1	N	0.3	50	41	$5s^2 19f$	$^2F°$	−49	3
Sn III $5s^2$ $^1S_0$	Limit		118 023.7	R	0.7						
$5s5p(^3P°)5d$	$^4D°$	1/2	119 981.1	R?	0.6	93	4	$5s5p(^3P°)5d$	$^4P°$	−116	2
$5s5p(^3P°)5d$	$^4D°$	3/2	120 064.3	R?	0.5	76	16	$5s5p(^3P°)5d$	$^4P°$	−73	2
$5s5p(^3P°)5d$	$^4D°$	5/2	120 253.6	R	0.3	52	39	$5s5p(^3P°)5d$	$^4P°$	54	3
$5s5p(^3P°)5d$	$^4D°$	7/2	122 491.5	R?	1.0	92	7	$5s5p(^3P°)5d$	$^4F°$	102	1
$5p^3$	$^4S°$	3/2	123 156.6	R	0.4	88	5	$5p^3$	$^2P°$	−2	4
$5s5p(^3P°)5d$	$^4P°$	5/2	123 688.2	N	0.5	55	41	$5s5p(^3P°)5d$	$^4D°$	60	2
$5s5p(^3P°)5d$	$^4P°$	3/2	124 245.66	R	0.20	80	18	$5s5p(^3P°)5d$	$^4D°$	15	8
$5s5p(^3P°)5d$	$^4P°$	1/2	124 524.6	N?	0.8	94	5	$5s5p(^3P°)5d$	$^4D°$	−13	1
$5s5p(^1P°)5d$	$^2D°$	3/2	132 168.83	R	0.24	51	32	$5p^3$	$^2D°$	−382	4
$5s5p(^1P°)5d$	$^2D°$	5/2	132 707.7	R	0.3	54	32	$5p^3$	$^2D°$	365	4

[a] Symbols next to the energy value have the following meaning: C—previous tentative identification has been confirmed here; N—new identification; R—previous value and/or interpretation has been revised here; ?—questionable identification.
[b] Uncertainties resulting from the level optimization procedure are given on the level of one standard deviation. They correspond to uncertainties of level separations from $5s^2 6p$ $^2P°_{3/2}$. To determine uncertainties of excitation energies from the ground level, the given values should be combined in quadrature with the uncertainty of the ground level, 0.05 cm^{-1}.
[c] The first percentage value refers to the configuration and term given in the first two columns of the table. The second percentage value refers to the configuration and term given next to it. The percentage compositions were determined in this work by a parametric least-squares fitting with Cowan's codes [30] (see text).
[d] Differences between observed energies and those calculated in the parametric least squares fitting.
[e] Number of observed lines determining the level in the optimization procedure.

McCormick and Sawyer [6]. Some of the transitions observed by McCormick and Sawyer were more accurately measured by Wu [11]. Brill [10] re-measured the 4f–6g transitions with much better accuracy. No discernible fine-structure splitting was detected in any of the observed $5s^2 ng$ ^2G multiplets. The lowest member of this series, $5s^2 5g$ ^2G, was unknown so far. Brill [10] observed a pair of lines at 9058.880 Å and 9063.658 Å with a separation 5.818(6) cm^{-1} closely matching his measured $5s^2 4f$ $^2F°$ $J = 5/2$–$7/2$ interval, 5.804 (9) cm^{-1}. He recognized that these lines must correspond to transitions combining the $5s^2 4f$ $^2F°_{5/2,7/2}$ levels with some unknown level, but he was unable to decide whether this level is located above or below $5s^2 4f$ $^2F°$. Thus, he gave two possible energy values for this unknown level, 78 258.194 (6) cm^{-1} or 100 324.103(6) cm^{-1}. By extrapolating the known energies of the $5s^2 ng$ ^2G terms with $n \geqslant 6$ to $n = 5$ with the core-polarization formula (see section 4.5), we found that the upper of these two suggested values almost exactly coincides with the predicted position of the $5s^2 5g$ ^2G term. Our LSF calculations ruled out the existence of a level at the lower of the two positions suggested by Brill, that could possibly combine with $5s^2 4f$ $^2F°$. Thus, we identified the level at 100 324.111(7) cm^{-1} as $5s^2 5g$ ^2G. Observed level energies and relative line intensities of all transitions from $5s^2 ng$ levels agree well with our calculations.

4.3. Optimization of energy levels

To derive the energy level values that best fit all observed transition wavelengths, we used the least-squares level optimization program LOPT [40]. The crucial factors for the level optimization procedure are the correct identification of the spectral lines, estimation of their uncertainties, and absence of systematic shifts. Correctness of identifications was ensured by the analysis described above. Estimation of the statistical and systematic uncertainties of wavelengths was described in section 3. This estimation partially relies on the level optimization procedure, since some of the reference wavelengths used in this procedure are the Sn II Ritz wavelengths. Therefore, the level optimization was made in several iterations. In the initial stage, only the accurate measurements of Brill [10], as well as our measurements in the VUV, for which independent estimates of uncertainties are available, were included in the optimization. This resulted in initial estimates of the energy levels and Ritz wavelengths derived from them. Deviations of wavelengths observed by Wu [11] and by McCormick and Sawyer [6] from these Ritz wavelengths revealed systematic shifts smoothly varying with wavelength. After these systematic shifts were removed, residual deviations of corrected wavelengths from Ritz values provided a sufficient statistical basis to assign uncertainties to all the measurements. Then the corrected wavelengths from Wu [11] and McCormick and Sawyer [6] were also included in the level optimization, leading to an extended and more accurate set of energy levels and Ritz wavelengths. This process was repeated until the estimated systematic shifts stopped changing.

The final list of optimized energy levels is given in table 3. In this table, the level uncertainties are given for separations from the $5s^26p\ ^2P°_{3/2}$ level. This level was chosen as the base, because it has the largest number of accurately measured transitions. To infer the uncertainty of an excitation energy from the ground level, one should combine the given uncertainty value in quadrature with the uncertainty of the ground level, 0.05 cm^{-1}. It can be seen that the level uncertainties vary greatly, from 0.003 cm^{-1} to 4 cm^{-1}, depending on the number and measurement accuracy of the lines determining the level. With a few exceptions, the level values are rounded using the 'rule of 24,' i.e., the uncertainty of the value does not exceed 24 units of the least significant digit of the value. In a few cases, an additional significant figure was required in order to reproduce the precisely measured transition wavelengths.

Twelve levels listed in table 3 have only one observed connecting line, as indicated in the last column. Four of them, $5s^26f\ ^2F°_{7/2}$ and three autoionizing levels, were already discussed in sections 4.2.2 and 4.2.3. The $5s^211s\ ^2S_{1/2}$ level, although it is based on only one transition to $5s^26p\ ^2P°_{3/2}$ observed by McCormick and Sawyer [6] at 2608.74 Å, is supported by the regular behavior of energies along the $5s^2ns$ series, as well as by good agreement of the observed intensity with our prediction. The remaining eight single-line levels are the members of the $5s^2ng$ series. As discussed in section 4.2.4, all these levels are actually unresolved terms with negligibly small $J = 7/2$–$9/2$ fine-structure intervals. Thus, to consider reliability of their identification, one should take into account all the lines observed from each ^2G term. Each of these terms, except $5s^211g$, is based on two distinct observed lines. These lines are the strongest predicted from these terms. Similar to the $5s^2ns$ series, all these identifications are confirmed by the regular behavior of energies and observed intensities along the series.

Some of the results of our LSF calculations, such as percentage compositions and differences of observed energies from those calculated in the parametric fitting are also given in table 3. The fitted parameter values obtained in the LSF are given in table 4.

Natural tin consists of ten stable isotopes with abundances ranging from 0.3% to 33%. Three of these isotopes have nuclear spin 1/2 and a rather large nuclear magnetic moment about $-1.0\,\mu_N$. Thus, lines observed from samples of natural tin (which were used in all experimental works quoted in the present paper) must be broadened by isotope shifts and hyperfine structure. Since there is no such entity as an atom of natural tin, the energy levels derived by our level optimization do not correspond to any physical object but are empirical values that best describe the observed spectral lines. This should be kept in mind when using the high-precision values from tables 1 and 3. Asymmetry of line profiles caused by isotope shifts and hyperfine structure may result in deviations of observed peak wavelengths from the Ritz values given in table 1. Observed isotope shifts between adjacent even isotopes are typically (0.005–0.02) cm^{-1}, while the hyperfine structure in less abundant odd isotopes is an order of magnitude larger. References to studies of isotope shifts and hyperfine structure of Sn II can be obtained from the NIST Atomic Energy Levels and Spectra Bibliographic Database at http://physics.nist.gov/Elevbib.

For completeness, we note that there is only one reported measurement of the Landé *g*-factor for Sn II. Namely, David *et al* [41] accurately measured the Landé *g*-factor for the $5s5p^2\ ^4P_{3/2}$ level to be 2.6609(7).

4.4. Intensities of observed lines

In the history of atomic spectroscopy, it has been an unfortunate long-standing tradition to give very rough estimates of relative intensities of observed lines. Although line intensities were always recognized to be important in correct identification of transitions causing them, the arguments had to be qualitative because the sensitivity of registration strongly varies with wavelength and depends on rarely quantified properties of detectors, spectrographs, and optics used. Also, different excitation conditions in light sources lead to large variations in line intensities. A method suggested and successfully used in a recent series of papers [42–44] overcomes these problems and allows one to reduce line intensities observed by different authors using different equipment to a common uniform scale. The method is based on using the Boltzmann equation to approximate populations of energy levels together with theoretically estimated radiative rates. It was shown in the papers quoted above that this approximation in most cases allows one to describe the observed intensities by a simple formula with weighted transition rate (gA) multiplied by a Boltzmann factor with a suitable effective excitation temperature. Then spectral response functions of the registration equipment can easily be derived by comparing observed and modeled intensities, and intensities observed with different setups can be reduced to a uniform scale with a common excitation temperature. Deviations of plasma conditions from the local thermodynamic equilibrium (LTE) and inaccuracies in estimated transition rates and derived response functions of registration equipment typically lead to errors of about a factor of three in such modeled intensities. Nevertheless, thus derived intensities provide a robust quantitative criterion for line identification and can even be used to estimate transition rates, when such estimates cannot be obtained from theory. Of course, the above-mentioned factor-of-three uncertainty is a restriction for many applications, but there are many cases where such estimates can be useful.

This method was applied to obtain the reduced relative intensities given in table 1. Below, we explain reduction of intensities for each set of observations.

The Boltzmann plot for our observed line intensities, shown in figure 3(a), indicates an effective excitation temperature of 2.0 eV in our triggered spark source. This plot was built with intensities corrected for the variation of response function of our equipment with wavelength, denoted as I_{corr}.

Table 4. LSF parameters (cm^{-1}) for Sn II.

Configuration	Parameter	LSF	Group[a]	STD	HFR	LSF/HFR
Odd parity[b]						
$5s^25p$	E_{av}	6860.3		116	0.0	
	$\zeta(5p)$	3016.3	1	83	2665.8	1.1315
…						
5s5p5d	E_{av}	128 129.4		152	117 237.6	1.0929
	$\zeta(5p)$	3415.7	1	94	3018.8	1.1315
	$\zeta(5d)$	77.2		Fixed	77.2	1.0000
	$F^2(5p5d)$	20 634.2		865	20 388.4	1.0121
	$G^1(5s5p)$	29 712.1	6	451	50 829.4	0.5845
	$G^2(5s5d)$	10 985.9		1189	9761.6	1.1254
	$G^1(5p5d)$	18 655.8	7	663	20 189.5	0.9240
	$G^3(5p5d)$	11 538.5	7	410	12 487.0	0.9240
$5p^3$	E_{av}	136 589.5		179	127 058.9	1.0750
	$F^2(5p5p)$	32 281.3		Fixed	37 046.5	0.8714
	$\zeta(5p)$	3064.7	1	84	2708.6	1.1315
$5p5d^2$[c]	E_{av}	262 609.7		Fixed	255 939.8	1.0261[c]
	$\zeta(5p)$	3732.4	1	103	3298.7	1.1315
…						
Even parity						
$5s5p^2$	E_{av}	63 956.0		36	55 474.7	1.1529
	$F^2(5p5p)$	32 090.9		286	36 826.8	0.8714
	$\zeta(5p)$	3040.9		57	2681.9	1.1339
	$G^1(5s5p)$	30 953.3		109	48 632.5	0.6365
…						
Configuration interaction[d]						
$5s5p^2$-$5s^25d$	$R^1(5p5p,5s5d)$	18 161.1	1	124	27 501.0	0.6604
$5s5p^2$-$5s^26d$	$R^1(5p5p,5s6d)$	9433.0	1	64	14 284.3	0.6604
…						

[a] Parameters in each numbered group were linked together with their ratio fixed at the Hartree–Fock level.
[b] All configuration-interaction parameters R^k for the odd configurations were fixed at 80% of the Hartree–Fock value.
[c] These highly excited configurations are unknown experimentally. They were included in the calculations in order to account for their interaction with other configurations studied in this work. Except for the average energies E_{av} given here and $\zeta(5p)$ for $5p5d^2$ and $4f5p^2$, all other parameters of these configurations were fixed at the 80% of the Hartree–Fock values (F^k, G^k, R^k) or 100% of the Hartree–Fock values (ζ).
[d] Other R^k parameters of the even configurations were fixed at 80% of the Hartree–Fock value.
(Only a portion of this table is shown here. The full table is given in the supplementary online material)

The logarithmic intensity-correction function $F(\lambda)$ used for this correction is shown in figure 3(b). Correction is made by multiplying the observed intensities by exponent of $F(\lambda)$. Transition rates gA used in the Boltzmann plots were calculated with Cowan's codes using our fitted parameters from the LSF.

Similarly, figures 3(c) and (d) present the Boltzmann plot and intensity-correction function for exposure 1 in Wu's line list [11]. It should be noted that the quantity given by Wu in the intensity columns is actually transparency (not the commonly used darkening) of the photographic plate on the scale 0–1000. To obtain the intensities, we subtracted his transparency values from 1000. Effective temperature in the source used for exposure 1 turned out to be 4.2 eV, which is the highest for all light sources used in the published literature. Apparently, this high temperature allowed Wu to observe lines from very highly excited levels not observed in other experiments. Reduction of intensities observed in the other three exposures reported by Wu [11] was made in a similar way. Effective temperatures for his exposures 2, 3, and 4 turned out to be about 3.6 eV, 3.7 eV, and 3.8 eV, respectively. Response functions derived from exposures 2 and 3, which cover the same wavelength range as exposure 1, are similar to the one shown in figure 3(d). For the final reduction of Wu's intensity values, we used the correction function averaged over these three exposures.

It should be noted that, despite the nonlinear properties of photographic plates, the original observed intensities in both our and Wu's work did not show any significant nonlinearity with exposure. This can easily be verified by plotting the ratio of calculated and observed intensities versus the observed intensity. Nonlinearity would result in a trend on such plots, which was not detected.

Intensities observed by Brill [10] and by McCormick and Sawyer [6] were reduced by the same method as described above. The effective excitation temperature in the light source

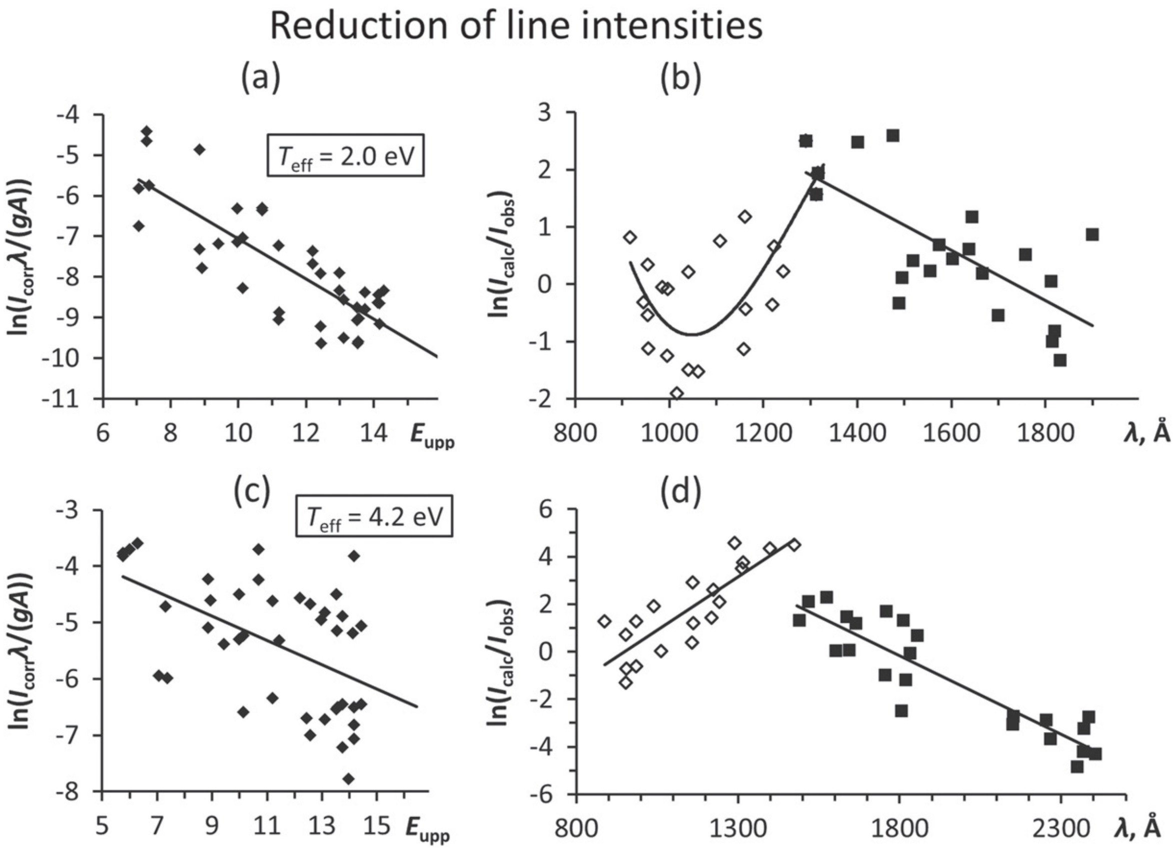

Figure 3. Boltzmann plots (a), (c) and logarithmic intensity-correction functions (b), (d) for our observations and those of Wu [11]. The upper-level energies E_{upp} in the Boltzmann plots are given in eV. The effective temperatures derived from the negative slope of the Boltzmann plots are shown in boxes. The calculated intensities I_{calc} in panels (b) and (d) are obtained from weighted transition rates gA calculated in the present work with a formula $I_{calc} = (gA/\lambda)\exp(-E_{upp}/T_{eff})$. Open diamonds and solid squares denote data points for separate wavelength ranges used to derive the linear or quadratic fits shown by solid lines.

used by Brill was found to be 1.9 eV, which is close to our triggered-spark value of 2.0 eV.

For the light source used by McCormick and Sawyer [6], the effective temperature was found to be somewhat lower, about 1.4 eV.

The values of effective excitation temperature given above are determined from Boltzmann plots which, as illustrated by figure 3, have a large scatter of data points. Thus, their accuracy is estimated as 20–40%. Effective excitation temperatures may differ from electron temperatures in the plasma. Rather than that, they approximately describe excitation conditions leading to the observed line intensities and can be used to reduce intensities from different light sources to a uniform scale that better represents relative intensities expected to occur in a single experiment.

After the variations of response functions of registration equipment were removed from the observed intensities, and the effective temperatures were determined for each set of observations, it was easy to scale the corrected observed intensities to the same effective temperature. We chose the highest temperature in all sets of measurements, 4.2 eV, as the basis for the unified scale. This choice is motivated by the need to have the smallest range of final intensity values, which is convenient for presentation purposes.

4.5. Ionization potential

The ionization potential (IP) given in AEL [4] is the value obtained by McCormick and Sawyer [6] using the $5s^2ng$ ($n = 6$–11) series. As the 5g level was established in the present work, and the measurements of McCormick and Sawyer contained significant systematic shifts, the IP has to be revised. We obtained the new value of IP using both the Ritz-type quantum-defect series extrapolation and core-polarization formula fitting for the $5s^2ng$ ^2G ($n = 5$–11) series using computer codes RITZPL and POLAR [45]; both leading to almost the same value. The formulas used in these series-fitting computer codes and explanation of their application can be found, for example, in [42]. The IP obtained from RITZPL using the two-parameter extended Ritz formula was 118 023.6(7) cm^{-1} and that from POLAR was 118 023.8 (7) cm^{-1}. Fitting of the three-parameter extended Ritz formula for the $5s^2ns$ ($n = 6$–11) series yields 118 036.3(2) cm^{-1} for the ionization energy. It is known that the ns series is slightly perturbed by an interaction with $5s5p^2$ $^2S_{1/2}$. The ng series is free from such perturbations. Therefore, we adopted the average IP value obtained from the two fits of the $5s^2ng$ series, 118 023.7(7) cm^{-1}, which is equivalent to 14.63 307 (8) eV. All fits were made using weights inversely proportional to squared uncertainties of the level values from table 2 combined in quadrature with the uncertainty of the ground level, 0.05 cm^{-1}. Our value is 6.7 cm^{-1} higher than the previously recommended value from McCormick and Sawyer [6].

5. Comparison with observed Auger electron spectrum

The Auger electron spectrum of Sn I and Sn II in the low-energy region 0–20 eV was observed by Forrest *et al* [46] in a crossed atomic and electron beams experiment. They assigned several observed peaks to autoionization decay of the $4d^95s^25p^2$ configuration of Sn II, not considered in this work. In addition, they tentatively assigned a strong peak observed at 2.529 eV to the autoionization decay of the $5p^3$ $^2P°$ term of Sn II. This assignment does not agree with our identifications. According to our parametric fitting, the $5p^3$ configuration is highly mixed with 5s5p5d, and the largest contribution of $5p^3$ $^2P°$ is predicted for the levels with large contributions from $5s5p(^3P°)5d$ $^2P°$ at about 128 000 cm^{-1} and $5s5p(^1P°)5d$ $^2P°$ at about 152 000 cm^{-1}. Autoionization decay of these levels to the $5s^2$ ground state of Sn III would produce Auger peaks at about 1.2 eV and 4.3 eV, respectively. Forrest *et al* [46] observed a weak peak at 1.023 eV and medium-strength peaks at 4.117 eV and 4.277 eV, which may be associated with these predicted levels. However, for the peak at 1.023 eV our calculations yield a higher autoionization rate from a close predicted $5s5p(^3P°)5d$ $^2F°_{5/2}$ level at about 127 000 cm^{-1}.

A few of the peaks observed by Forrest *et al* [46] closely match the experimental energies of autoionizing Sn II levels we derived from our observed optical spectrum. In particular, the peaks observed at 1.761 eV and 1.829 eV closely match the predicted Auger energies for the $5s5p(^1P°)5d$ $^2D°$ $J = 3/2$ and 5/2 levels (observed at 132 168.83 cm^{-1} and 132 707.7 cm^{-1}), respectively.

The peak observed at 0.657 eV can be a blend of Auger decays of the $5p^3$ $^4S°_{3/2}$ and $5s5p(^3P°)5d$ $^4P°_{5/2}$ levels (which we observed at 123 156.6 cm^{-1} and 123 688.2 cm^{-1}, respectively). These decays are predicted to be of comparable strengths, due to small admixtures of doublet terms in the composition of these levels.

The peak at 0.285 eV was assigned by Forrest *et al* [46] to the decay of the Sn I $5s5p^3$ $^3P°_1$ level to the $5s^25p$ $^2P°_{1/2}$ ground level of Sn II. However, this assignment was later rejected by Dembczynski and Wilson [47]. This peak closely matches our observed energy for the Sn II $5s5p(^3P°)5d$ $^4D°_{5/2}$ level (120 253.6 cm^{-1}, corresponding to the Auger electron energy of 0.2773 eV), while the observed peak at 0.523 eV matches the decay of the $5s5p(^3P°)5d$ $^4D°_{7/2}$ level (122 491.5 cm^{-1}, corresponding to the Auger electron energy of 0.5548 eV).

Finally, our calculations predict the metastable $5s5p(^3P°)5d$ $^4F°_{9/2}$ level at 118 700 cm^{-1}. Autoionization of this level should produce an Auger peak at ejected electron energy of 0.088 eV. The strongest peak observed by Forrest *et al* [46] is at 0.053 eV. This peak may be due to the decay of this metastable level.

We note that autoionization rates calculated for the Sn II levels discussed in this section are unreliable, because they strongly depend on very small mixing between doublet and quartet levels and on poorly known interaction between the $5p^3$ and 5s5p5d configurations. This, as well as the low resolution of the observed Auger electron spectrum [46], precludes definite identification of the observed Auger features. More sophisticated calculations, as well as higher-resolution experiments, are needed to elucidate the structure of autoionizing Sn II levels in the region just above the first ionization limit.

6. Transition probabilities

Oliver and Hibbert [14] made a large-scale Breit–Pauli configuration-interaction (CI) calculation of transition probabilities of Sn II using the CIV3 code of Hibbert and coworkers (see references in [14]). They presented three sets of results: one for their *ab initio* calculation (in the length gauge) and two for the fine-tuned calculation (one in the length gauge and the other in the velocity gauge). The fine tuning consisted of semiempirical adjustment of the diagonal matrix elements of the Hamiltonian minimizing the differences between the calculated and experimental eigenvalues. The line strengths S_L obtained in the length gauge in the fine-tuned calculation are considered to be the most accurate ones from the three sets. Their accuracy can be assessed by comparing them with the other two data sets, S_v (fine-tuned, velocity gauge) and S_{ab} (*ab initio*, length gauge). This comparison, illustrated in figure 4, shows that for strong lines with $S_L > 0.28$ the length and velocity forms of line strength agree within 6% on average, while for weaker lines with $S_L = (0.03–0.28)$ the agreement is somewhat worse, about 12% on average. We adopted these standard deviations as conservative estimates of uncertainties of S_L in the corresponding ranges of line strength.

For the ten weakest lines with $S_L < 0.03$, the length and velocity forms strongly disagree with each other. Most of these transitions are intercombination ones between doublet and quartet levels. As pointed out by Oliver and Hibbert [14], for such transitions, calculation of the line strength in velocity gauge requires additional terms not accounted for in the CIV3 code. This makes the comparison meaningless for intercombination transitions. Instead, the comparison of the *ab initio* and fine-tuned calculations in the length gauge can be used for estimating their uncertainties. Except for one large deviation for the $5s^25p$ $^2P°_{3/2} – 5s5p^2$ $^2S_{1/2}$ transition at 1394.667 Å, S_{ab} agrees with S_L within 12%. However, because of low statistics, we adopt a conservative estimate of 35% for the uncertainty of transitions with $S_L = (0.001–0.03)$ and omit the three weakest transitions, for which the transition rate given by Oliver and Hibbert [14] strongly contradicts the observed line intensities.

The high accuracy of calculations of Oliver and Hibbert [14] for strong lines is further confirmed by comparison of

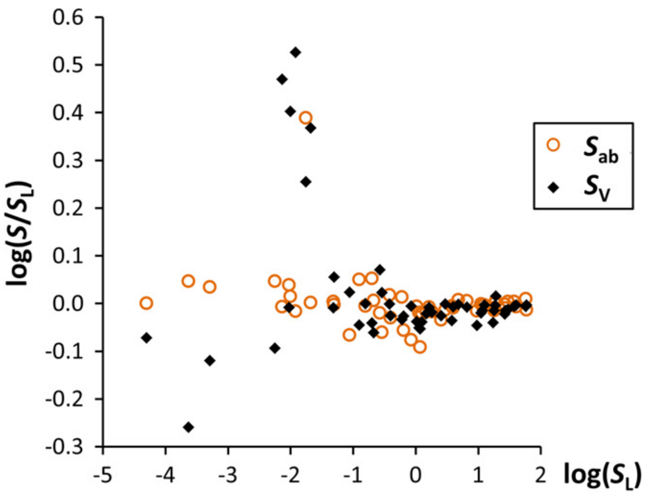

Figure 4. Comparison of line strengths S calculated by Oliver and Hibbert [14] in different approximations and gauges: S_L—fine-tuned calculation in length gauge; S_V—fine-tuned calculation in velocity gauge; S_{ab}—*ab initio* calculation in length gauge.

calculated and observed radiative lifetimes presented in table 5.

David *et al* [41], employing the direct magnetic resonance method, measured the lifetime of the $5s5p^2\ ^4P_{1/2}$ level in Sn II to be 325(40) ns. They supported this result by two additional less accurate measurements with two independent methods.

Schectman *et al* [15] measured the lifetimes of three levels, $5s^25d\ ^2D_{3/2,5/2}$ and $5s^24f\ ^2F°_{5/2}$, with a beam-foil method. Using a similar method, Andersen and Lindgård [16] measured the lifetime of the $5s^26s\ ^2S_{1/2}$ and $5s^25d\ ^2D_{3/2}$ levels. Both these studies carefully accounted for effects of cascades on the measured decay curves.

Gorshkov and Verolainen [51] determined the lifetimes of the two $5s^24f\ ^2F°_{5/2,7/2}$ levels by using intersecting atomic and electron beams and a multichannel method of retarded coincidences. Although they reported very small uncertainties of ±0.5 ns, their description of the experiment lacks any mention of an account for cascading effects. Therefore, in table 5 we have doubled their uncertainty estimate.

As can be seen from table 5, lifetimes calculated by Oliver and Hibbert [14] agree with all the best measurements within the uncertainties.

Our own calculations made with the Cowan codes (using the LSF parameters) are compared with the calculations of Oliver and Hibbert [14] in figure 5.

For strong transitions with line strength $S > 0.5$, our calculations agree with those of Oliver and Hibbert [14] to 28% on average. For weaker transitions, the results of Cowan's codes deviate from Oliver and Hibbert [14] by more than a factor of two on average. Calculations of Alonso-Medina *et al* [50], also using a parametric fitting with Cowan's codes, are of similar quality, although they display somewhat larger deviations from Oliver and Hibbert [14] (about 30% on average for $S > 1$, and 70% for weaker transitions). We note that the *f*- and *A*-values given by Alonso-Medina *et al* [50] in their table V for the $5s^2nf$–$5s^2n'g$ transitions are not consistent with each other and strongly disagree with our calculations.

Results of Oliver and Hibbert [14] also compare well with the relativistic all-order calculations of Safronova *et al* [52]. These authors presented their results only for a few $5s^2ns$–$5s^2n'p$ and $5s^2np$–$5s^2n's$ transitions. They agree with Oliver and Hibbert [14] with an average deviation of 12%, except for one $5s^25p\ ^2P°_{3/2} - 5s^27s\ ^2S_{1/2}$ transition (1219.088 Å), for which their S value is lower by a factor of 2.5.

Aside from a few discrepancies mentioned above, theoretical calculations of line strengths agree with each other, at least for strong transitions, and they agree reasonably well with the few available lifetime measurements. However, comparison with experimentally measured radiative rates (*A*-values) presents problems. The *A*-values were measured for several tens of transitions by Alonso-Medina and Colón [48], Schectman *et al* [15], Miller *et al* [53], Wujec and Weniger [54], and Wujec and Musielok [55]. Experimental line strengths reported in these papers are compared with the critically evaluated theoretical data in figure 6. Only a few measured values agree with theory within the claimed measurement uncertainties. The greatest discrepancies are observed for the weakest lines measured by Alonso-Medina and Colón [48]. It is difficult to identify the causes of the discrepancies. However, from the above analysis of the theoretical data, we conclude that the discrepancies originate in some flaws in the measurements. For this reason, we retained in table 1 only four experimental *A*-values, three from Alonso-Medina and Colón [48] and one from Miller *et al* [53], and assigned greatly increased uncertainties to them.

We included in table 1 four lines at 2442.7 Å, 2486.6 Å, 2592.3 Å, and 3351.3 Å, for which Alonso-Medina and Colón [48] reported measured *A*-values. Since these authors did not attempt to accurately measure the wavelengths, and these lines were not reported by other authors, the wavelengths given in the column λ_{obs} are actually the rounded Ritz wavelengths. We note that the last two of these lines, as well as two other lines reported by Alonso-Medina and Colón [48] at 2592.6 Å and 3351.9 Å, were incorrectly identified by these authors.

We also included in table 1 one unobserved parity-forbidden line corresponding to the transition between the levels of the ground term. Our predicted wavelength for this far-infrared line is 23 521.14(24) Å. According to calculations of Biémont *et al* [49], Warner [56], and Garstang [57], this line is dominated by the magnetic dipole (M1) transition. The *A*-values calculated for this M1 transition in these works agree with each other within 1%. The *A*-value for the electric quadrupole transition, 2.893 s^{-1} [49], amounts to only 0.4% of the M1 decay rate and can be neglected in most applications.

Since the statistical distribution of both measured and calculated *A*-values is far from normal, uncertainties of the adopted *A*-values are specified in table 1 with a letter code instead of numerical values. The letter code is explained in table 6.

Table 5. Comparison of observed and calculated lifetimes in Sn II.

Level		Energy (cm^{-1})	τ_{obs} (ns)	Reference[a]	τ_{th} (ns)	Reference[a]
5s5p^2	$^4P_{1/2}$	46 464.290	325(40)	D80	375	OH10
			1500[b]	AM00	215	TW
					237	AM05
5s^{2}6s	$^2S_{1/2}$	56 886.363	1.10(10)	AL77	1.16	OH10
					1.20	TW
					1.13	AM05
5s^{2}5d	$^2D_{3/2}$	71 406.142	0.44(2)	S00	0.45	OH10
			0.50(5)	AL77	0.37	TW
					0.41	AM05
5s^{2}5d	$^2D_{5/2}$	72 048.260	0.46(4)	S00	0.51	OH10
					0.45	TW
					0.50	AM05
5s^{2}4f	$^2F^\circ_{7/2}$	89 288.255	5.0(10)[c]	GV85	3.82	OH10
			6.9[b]	AM00	3.28	TW
					3.21	AM05
5s^{2}4f	$^2F^\circ_{5/2}$	89 294.055	4.6(10)	S00	3.78	OH10
			5.2(10)[c]	GV85	3.24	TW
			4.8[b]	AM00	3.04	AM05

[a] References: AL77—Andersen and Lindgård [16]; AM00—Alonso-Medina and Colón [48]; AM05—Alonso-Medina *et al* [50] (Cowan code); D80—David *et al* [41]; GV85—Gorshkov and Verolainen [51]; OH10—Oliver and Hibbert [14]; S00—Schectman *et al* [15]; TW—this work (Cowan code).
[b] Determined from the sum of measured radiative rates.
[c] Original estimate of uncertainty doubled (see text).

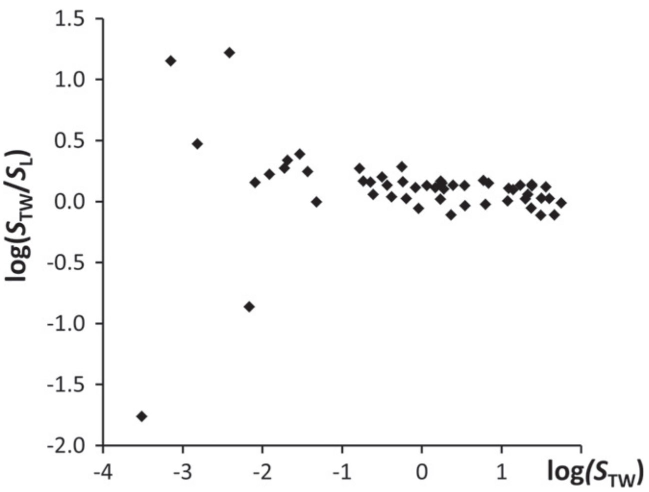

Figure 5. Comparison of line strengths calculated in the present work with Cowan's codes (S_{TW}) with those from fine-tuned calculations of Oliver and Hibbert [14] in the length gauge (S_L).

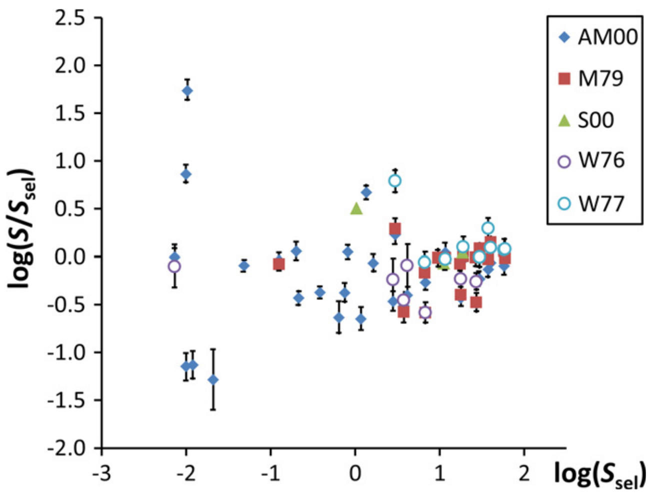

Figure 6. Comparison of experimental line strengths S with selected theoretical data. The selected line strength S_{sel} were taken from Oliver and Hibbert [14] and from our calculations and have estimated uncertainties between 6% and 35%. The error bars correspond to claimed measurement uncertainties (one standard deviation). Key to experimental work: AM00—Alonso-Medina and Colón [48]; M79—Miller *et al* [53]; S00—Schectman *et al* [15]; W76—Wujec and Musielok [55]; W77—Wujec and Weniger [54].

7. Conclusion

A comprehensive interpretation of the spectrum of singly ionized tin (Sn II) is presented here. The analysis covers the wavelength region 888–10 740 Å. The earlier reported levels of even parity configurations, 5s^2*n*d (n = 5–11), 5s^2*n*s (n = 6–11), 5s^2*n*g (n = 6–11) and 5s5p^2 have been confirmed with minor improvements in their level values, while the 5s^{2}5g level has been newly identified. The questions in the assignments of the $^2S_{1/2}$ and $^2P_{1/2}$ levels of the 5s5p^2 configuration have been resolved. In odd parity, the previously

Table 6. Transition probability uncertainty code.

Letter	Uncertainty in *A*-value	Uncertainty in log(*gf*)
AAA	⩽0.3%	⩽0.0013
AA	⩽1%	⩽0.004
A+	⩽2%	⩽0.009
A	⩽3%	⩽0.013
B+	⩽7%	⩽0.03
C+	⩽18%	⩽0.08
C	⩽25%	⩽0.11
D+	⩽40%	⩽0.18
D	⩽50%	⩽0.24
E	>50%	>0.24

reported levels of the $5s^2np$ ($n=5$–9) and $5s^2nf$ ($n=4$–6) configurations have been verified. Sixty-nine levels are now known in Sn II. Among these, eight are new, and for 11 levels previous values and/or interpretations have been revised. The level values, which are based on the identification of about 200 spectral lines, have been optimized in a LSF procedure. About 70 of these lines were measured by us either for the first time or with a significantly improved precision. With these improved data, the ionization energy of Sn II has been determined more accurately. For 140 transitions out of total 215, we give a critically evaluated value of transition probability with an estimated uncertainty. About 40% of these transition probabilities have an accuracy C+ (⩽18%) or better.

Acknowledgements

KH would like to duly acknowledge the Council of Scientific and Industrial Research (CSIR) for giving financial support through the Senior Research Fellowship (SRF) Scheme. AT is thankful to the kind hospitality of late Prof. Y N Joshi and St. Francis Xavier University, Antigonish (Canada) during the recording of tin spectra.

References

[1] Hobbs L M, Welty D E, Morton D C, Spitzer L and York D G 1993 *Astrophys. J.* **411** 750
[2] Sofia U J, Meyer D M and Cardelli J A 1999 *Astrophys. J.* **522** L137
[3] Foster A R, Counsell G F and Summers H P 2007 *J. Nucl. Mater.* **363** 152
[4] Moore C E 1958 *Atomic Energy Levels, National Bureau of Standards Circular 467* vol 3 (Washington, DC: US Govt. Printing Office)
[5] Kramida A, Ralchenko Y and Reader J and NIST ASD Team 2012 *NIST Atomic Spectra Database, v.5.0* (Gaithersburg, MD: National Institute of Standards and Technology) (http://physics.nist.gov/ASD)
[6] McCormick W W and Sawyer R A 1938 *Phys. Rev.* **54** 71
[7] Green J B and Loring R A 1927 *Phys. Rev.* **30** 574
[8] Narayan A L and Rao K R 1927 *Nat. Commun.* **120** 120
[9] Lang R J 1930 *Phys. Rev.* **35** 445
[10] Brill W G 1964 The arc spectrum of tin *PhD Thesis* Purdue University, Lafayette, IN, USA
[11] Wu C M 1967 The atomic spark spectra of tin, Sn III, Sn IV, Sn V *Master Thesis* University of British Columbia, Canada
[12] Lysaght M A, Kilbane D, Cummings A, Murphy N, Dunne P, O'Sullivan G, Kampen P van, Costello J T and Kennedy E T 2005 *J. Phys.* B **38** 4247
[13] Duffy G, van Kampen P and Dunne P 2001 *J. Phys. B: At. Mol. Opt. Phys.* **34** 3171
[14] Oliver P and Hibbert A 2010 *J. Phys. B: At. Mol. Opt. Phys.* **43** 074013
[15] Schectman R M, Cheng S, Curtis L J, Federman S R, Fritts M C and Irving R E 2000 *Astrophys. J.* **542** 400
[16] Andersen T and Lindgård A 1977 *J. Phys. B: At. Mol. Opt. Phys.* **10** 2359
[17] Alonso-Medina A, Colón C and Martínez H C 2003 *Astrophys. J.* **595** 550
[18] Kaufman V and Edlén B 1974 *J. Phys. Chem. Ref. Data* **3** 825
[19] Glad S 1954 *Ark. Fys.* **7(2)** 7
[20] Edlén B 1963 *Rep. Prog. Phys.* **26** 181
[21] Bockasten K 1955 *Ark. Fys.* **9(30)** 457
[22] Griesmann U and Kling R 2000 *Astrophys. J.* **536** L113
[23] Eriksson K B S 1987 *J. Opt. Soc. Am.* B **4** 1369
[24] Edlén B 1934 *Nova Acta Reg. Soc. Sci. Upsalien., Ser. IV* **9(6)** 1
[25] Bromander J 1969 *Ark. Fys.* **40(23)** 257
[26] Kaufman V and Hagan L 1979 *J. Opt. Soc. Am.* **69** 232
[27] Toresson Y G 1961 *Ark. Fys.* **18(28)** 389
[28] Brown C M, Tilford S G and Ginter M L 1977 *J. Opt. Soc. Am.* **67** 607
[29] Bhatia K S 1969 Analysis of doubly and triply ionised indium *PhD Thesis* University of British Columbia, Canada
[30] Cowan R D 1981 *The Theory of Atomic Structure and Spectra* (Berkeley, CA: University of California Press) and Cowan code package for Windows by A K Kramida available from (http://das101.isan.troits.ru/COWAN)
[31] Sansonetti J E and Martin W C 2005 *J. Phys. Chem. Ref. Data* **34** 1559
[32] Connerade J P and Baig M A 1981 *J. Phys. B: At. Mol. Opt. Phys.* **14** 29
[33] Colón C and Alonso-Medina A 2004 *Astron. Astrophys.* **422** 1109
[34] Garton W R S, Parkinson W H and Reeves E M 1966 *Can. J. Phys.* **44** 1745
[35] Kaufman V, Sugar J and Joshi Y 1988 *J. Opt. Soc. Am.* B **5** 619
[36] Kaufman V and Sugar J 1987 *J. Opt. Soc. Am.* B **4** 1924
[37] Tauheed A, Joshi Y N and Rana T 2000 *Phys. Scr.* **61** 696
[38] Tauheed A, Zafaran A F and Joshi Y N 1999 *J. Phys. B: At. Mol. Opt. Phys.* **32** 2917
[39] Tauheed A, Joshi Y N and Pinnington E H 1998 *J. Phys. B: At. Mol. Opt. Phys.* **31** 393
[40] Kramida A E 2011 *Comput. Phys. Commun.* **182** 419
[41] David D, Hamel J and Barrat J-P 1980 *Opt. Commun.* **32** 241
[42] Kramida A 2013 *Fusion Sci. Technol.* **63** 313
[43] Kramida A 2013 *J. Res. Natl. Inst. Stand. Technol.* **118** 52
[44] Kramida A 2013 *J. Res. Natl. Inst. Stand. Technol.* **118** 168
[45] Sansonetti C J 2005 *Computer programs RITZPL and POLAR*, private communication
[46] Forrest L F, James G K, Ross K J, Wilson M and Pantinakis A 1985 *J. Phys. B: At. Mol. Opt. Phys.* **18** 3123
[47] Dembczynski J and Wilson M 1988 *Z. Phys.* D **8** 329
[48] Alonso-Medina A and Colón C 2000 *Phys. Scr.* **61** 646
[49] Biémont E, Hansen J E, Quinet P and Zeippen C J 1995 *Astron. Astrophys. Suppl. Ser.* **111** 333
[50] Alonso-Medina A, Colón C and Rivero C 2005 *Phys. Scr.* **71** 154

[51] Gorshkov V N and Verolainen Ya F 1985 *Opt. Spectrosc.* **59** 694
[52] Safronova U I, Safronova M S and Kozlov M G 2007 *Phys. Rev.* A **76** 022501
[53] Miller M H, Roig R A and Bengtson R D 1979 *Phys. Rev.* A **20** 499
[54] Wujec T and Weniger S 1977 *J. Quant. Spectrosc. Radiat. Transfer* **18** 509
[55] Wujec T and Musielok J 1976 *Astron. Astrophys.* **50** 405
[56] Warner B 1968 *Z. Astrophys.* **69** 399
[57] Garstang R H 1964 *J. Res. Natl. Bur. Stand.* A **68** 61